AN ABSTRACT OF THE THESIS OF

Sean W. Fleming for the degree of Master of Science in Geophysics presented on December 12, 1996. Title: Bulldozer Blades and Colliding Submarine Mountain Chains: Constraints on Central Oregon Convergent Margin Tectonics from Magnetics and Gravity.

Redacted for Privacy

Abstract Approved: _____

Anne M. Trehu

Magnetic and gravity modelling was completed along two E-W transects offshore central Oregon. These models indicate that the backstop-forming western edge of the Siletz terrane has a seaward dip of approximately 40° to 49° at 44°48'N, shallowing to ~28° at 44°11'N. This is a well-determined result, given available a priori information, to a depth of ~7 km. The edge of the Siletz terrane may continue to descend at these dips to the JdF plate, but alternate geometries for the lowermost portion of the backstop are also consistent with the potential field data. The magnetic data also require progressive eastward demagnetization of the subducting JdF crust, which is most likely due to heating of the descending oceanic plate to the Curie temperature. Our southern transect reveals that Heceta Bank is cored by relatively high-density sediments (~2.54 g/cc), consistent with the model proposed by Kulm and Fowler (1974) for submarine bank formation in the Oregon convergent margin. On the basis of magnetic, gravity, and velocity data, we tentatively interpret a deeply buried, linear aseismic ridge to be present beneath the accretionary complex from about 45°N to

42°N. This ridge may collide with the backstop beneath Heceta Bank and may play a role, in concert with imbricate thrust faulting, in the formation of Heceta Bank's high-density core. We also speculate that differences in depth to the JdF plate due to juxtaposition of different-aged crust across pseudofaults which intersect the coast at Nehalem and Heceta Banks may be a factor in the construction of these topographic highs.

Bulldozer Blades and Colliding Submarine Mountain Chains: Constraints on Central Oregon Convergent Margin Tectonics from Magnetics and Gravity

by

Sean W. Fleming

A THESIS

submitted to

Oregon State University

in partial fulfillment of
the requirements for the
degree of

Master of Science

Presented December 12, 1996
Commencement June 1997

Master of Science thesis of Sean W. Fleming presented on December 12, 1996

APPROVED:

Redacted for Privacy

Major Professor, representing Geophysics

Redacted for Privacy

Dean of College of Oceanic and Atmospheric Sciences

Redacted for Privacy

Dean of Graduate School

I understand that my thesis will become part of the permanent collection of Oregon State University libraries. My signature below authorizes release of my thesis to any reader upon request.

Redacted for Privacy

Sean W. Fleming, Author

ACKNOWLEDGEMENTS

First and foremost, I would like to thank my advisor, Anne Trehu, for supporting me throughout the course of my research. I also would like to extend my gratitude to all the researchers at the College of Oceanic and Atmospheric Sciences and the O.S.U. Geosciences Department who shared their valuable knowledge and experience with me, including (in alphabetical order): John Chen, Dave Christie, Chris Goldfinger, Roy Haggerty, Vern Kulm, Shaul Levi, Bob Lillie, John Nabalek, and Bob Yates. Special thanks go out to my committee members for their time and effort: Anne Trehu, Vern Kulm, John Chen, and Jennifer Field. I received a great deal of both moral and intellectual support from my fellow grad students, including Jochen Braunmiller, Charlie Hutto, Beatte Leitner, Xiao-Qing Li, Lisa McNeill, Maren Scheidhauer, Bernd Schurr, and Weerachai Siripunvaraporn, and a very special thanks goes out to Christof Lendl, who provided an enormous amount of help with smoothing over the technical difficulties. I would also like to thank Jerry Connard at Northwest Geophysical Associates and the "computer guys" at C.O.A.S. for their technical support, and for not openly laughing at dumb questions. I wish also to acknowledge the (mostly successful, I think) efforts of my teachers at the University of British Columbia and my supervisors and coworkers at Pacific Geophysical, J. Arthur and Associates, Numac Energy, Mobil Oil Canada, and Shell Canada to instill in me both an interest in geophysics and a solid background in the field.

I also wish to thank my family, especially my mother, Alice Fleming, as well as my girlfriend, Kristine Penn, for their support.

An additional debt of gratitude is owed to the American taxpayer, who made it all possible. This work was supported by the USGS-NEHRP program under agreements 1434-95-G-2617 and 1434-95-G-2636.

TABLE OF CONTENTS

Page

1. INTRODUCTION 1

2. GEOLOGIC FRAMEWORK 6

2.1 The Siletz Terrane 6

2.2 Morphology of the Oregon Continental Margin and Neotectonics 13

3. POTENTIAL FIELD DATA 19

4. MODELLING 21

4.1 North Line, 44°48'N 21

4.1.1 Model Geometry 22
4.1.2 Model Parameterization 23
4.1.3 Modelling Results 28

4.2 South Line, 44°11'N 47

4.2.1 Model Geometry and Parameterization 47
4.2.2 Modelling Results 52

5. DISCUSSION 57

5.1 Backstop Geometry, Accretionary Prism Deformation, Stress Fields, and Theoretical Models of Forearc Deformation: A Synthesis 57

5.2 Heceta Bank 61

6. CONCLUSIONS 67

BIBLIOGRAPHY 69

APPENDIX 76

Appendix: Computational Basis for Magnetics and Gravity Modelling 77

LIST OF FIGURES

Figure — Page

1. Location map 2

2. Seismic velocity model of Trehu et al. (1994), coincident with and an important constraint to our model of the northern transect 3

3a. NOAA shiptrack locations and magnetics along track, over National Geophysical Data Center (NGDC) 2D magnetics and bathymetry 7

3b. NOAA shiptrack locations and free-air gravity along track, over NGDC 2D gravity and bathymetry 9

4. Simplified neotectonic map 14

5. Migrated MCS reflection line of Trehu et al. (1995) 16

6. Potential field model of Oregon convergent margin at 44°48'N (north line) ... 29

7. Magnetics along track, north line 33

8. Contour plot of RMS error as a function of dip of the Siletz edge and bulk susceptibility of the Siletz terrane 37

9. Examples of acceptable backstop models, north line 38

10. Plot of densities of discrete bodies in our potential field model of the north line (figure 6) against corresponding range of velocities from nondiscretized velocity model (figure 2) 41

11. 3D plot of NGDC magnetic data in narrow N-S strip along Oregon convergent margin, illuminated from W, viewed from SW 43

12. Potential field model of Oregon convergent margin, 44°11'N (south line) 48

13. Comparison of observed gravity anomaly to that predicted by three preliminary models 54

LIST OF TABLES

Table — Page

1. Model parameters for north line (figure 6) 31

2. Model parameters for south line (figure 12) 50

Bulldozer Blades and Colliding Submarine Mountain Chains: Constraints on Central Oregon Convergent Margin Tectonics from Magnetics and Gravity

1. INTRODUCTION

Oceanic crust of the Juan de Fuca (JdF), Gorda, and possibly Explorer plates, all remnants of the Farallon plate, is obliquely subducted beneath the continental crust of the North American (NA) plate from the Mendocino Triple Junction in Northern California to either the southern or northern margin of the Explorer plate, offshore southwestern British Columbia (Rohr and Furlong, 1995) (figure 1). The Cascadia subduction zone has a shallow angle of subduction and a thick accretionary prism (figure 2). It is unusual in that no historical or instrumental record of great subduction earthquakes exists and even small earthquakes on the plate boundary are very rare. However, geodynamic considerations (Heaton and Kanamori, 1984) suggest that the Cascadia megathrust should be seismogenic, and paleoseismological evidence (Atwater, 1987) indicates that large earthquakes have struck the region in the past, with the most recent event probably having occured about 300 years ago.

Recent studies suggest the importance of heterogeneities in upper and lower plate structure to the distribution of earthquakes (e.g. Trehu et al., 1994, Dmowska et al., 1996). Upper and lower plate seismicity is also anomalous in Cascadia, showing a very heterogenous distribution. Earthquake activity is common in Washington and near the Mendocino triple junction (e.g. Shedlock and Weaver, 1991), but is

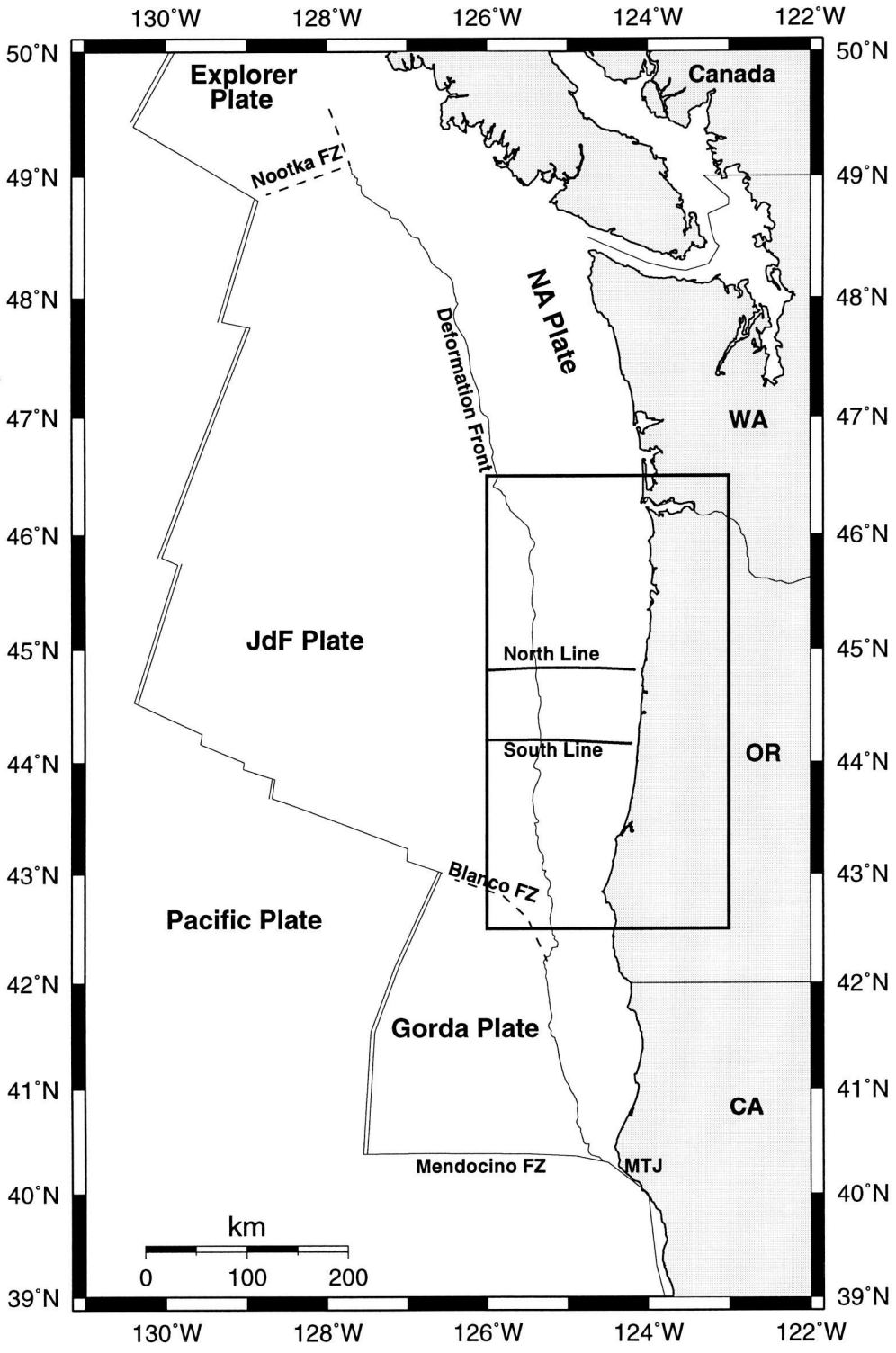

Figure 1. Location map. Positions of two potential field transects of this study are shown. Box indicates area shown in Figure 3. JdF=Juan de Fuca, NA=North America, FZ=fracture zone, MTJ=Mendocino Triple Junction.

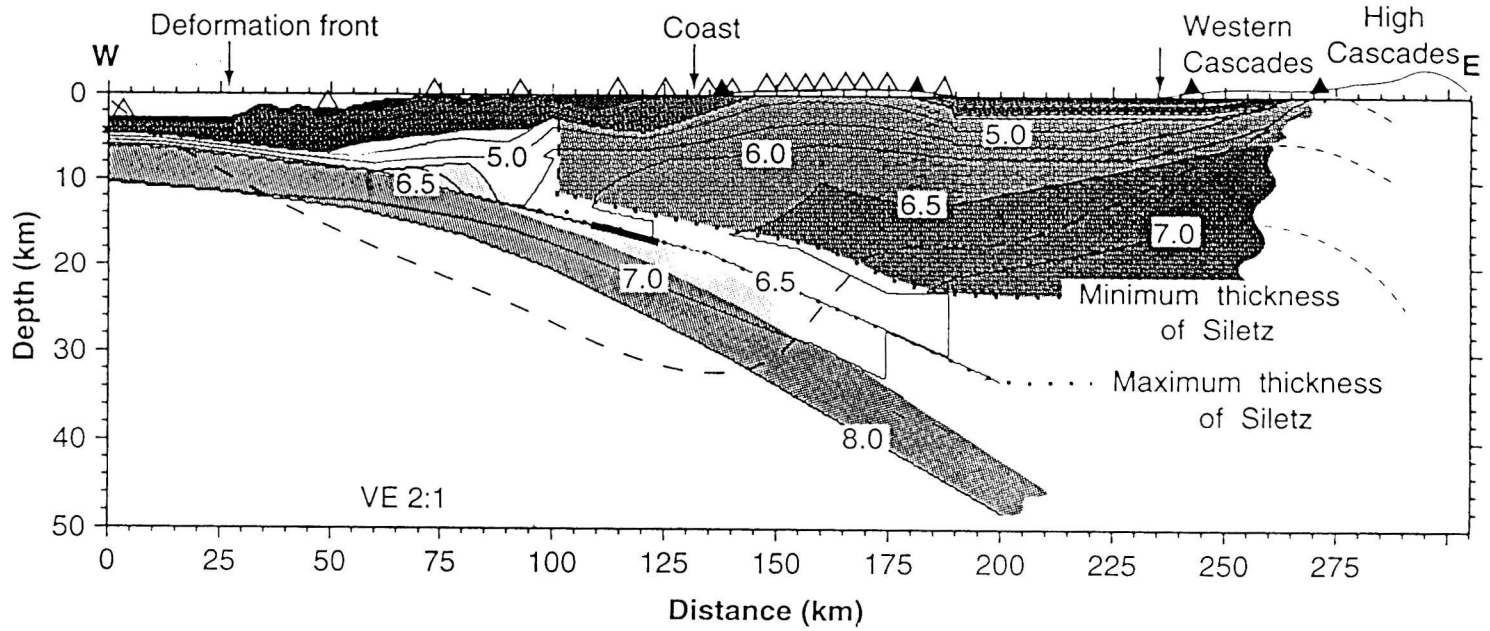

Figure 2. Seismic velocity model of Trehu et al. (1994), coincident with and an important constraint to our model of the northern transect. Contour interval is 0.5 km/s. V.E. = 2. Bold line at 110 to 125 km indicates a deep reflection interpreted to indicate base of Siletzia or top of subducted oceanic crust. Bold dashed line at about 100 km shows position of seaward edge of Siletz terrane as inferred by Trehu et al. (1994). Note that distance axis is shifted 15.9 km to the east relative to distance axis of our potential field model of the north line (figure 6).

dramatically absent in central and southern Oregon. This distribution of crustal seismicity generally correlates with variations in the thickness of the Siletz terrane, which forms the basement over much of the region (Trehu et al., 1994). Changes in deformational style in the accretionary prism (e.g. Goldfinger et al., 1992, Goldfinger et al., in press, McNeill et al., submitted, Charles Hutto, pers. com., 1996) also correlate well with variations in the structure and the location of the edge of the Siletz terrane (Snavely, 1987, Trehu et al., 1994; see figure 4), which may be acting as the subduction zone backstop (Duncan, 1982, Trehu et al., 1994).

A backstop may be defined as a region within a forearc that has significantly greater shear strength than trenchward sediments, and which thus acts as a bulldozer blade driving the accretionary wedge (Byrne et al., 1993, Davis et al., 1983). Differing backstop geometries produce different stress and strain fields within an accretionary prism (Byrne et al., 1993), and the dynamics of sediment subduction, melange formation, and prism accretion are in part a function of the geometry and properties of the overriding plate, including the backstop (Shrieve and Cloos, 1986, von Huene et al., 1996). The geometry of the backstop thus helps to determine subduction zone dynamics and is a fundamental consideration in earthquake hazard assessment; this is particularly true along the Oregon continental margin, where the distribution of seismicity and changes in deformational style visibly correlate with the distribution and nature of the backstop. In addition, thermal models of the Cascadia subduction zone are sensitive to the geometry and extent of the low thermal conductivity basalts of the Siletz terrane (Hyndman and Wang, 1993,

Oleskevich, 1994); accurate thermal modeling is critical to predicting the size of the locked zone and thus the magnitude of megathrust earthquake that can be expected.

A potential field modelling effort was undertaken on the central Oregon continental margin to develop a better understanding of the geometry of the seaward edge of the Siletz terrane. Marine magnetics and gravity data were considered along E-W lines at two latitudes: 44°48'N, where a recent seismic imaging experiment provides strong constraints on crustal structure, and 44°11'N, crossing an enigmatic topographic high known as Heceta Bank.

2. GEOLOGIC FRAMEWORK

2.1 The Siletz Terrane:

Continental basement over much of Oregon and Washington west of the Cascade volcanic arc consists of an accreted block of oceanic basalt known variously as the Siletz terrane, Crescent terrane, and Siletzia. The rocks of the Siletz terrane are locally known as the Roseburg Fm., Siletz River Volcanics, Crescent Fm., and Metchosin Volcanics (Snavely, 1987). It is technically difficult to identify a subsurface contact between crystalline basement and slightly younger, overlying volcanic rocks, and Duncan (1982) also chose to include the younger Grays River and Tillamook Volcanics as Siletz terrane rocks. It is sufficient for our purposes to refer to the backstop-forming crystalline basement as a whole as the Siletz terrane.

Siletzia terminates against the pre-Tertiary Klamath terrane to the south. To the east, gravity and refraction studies show that Siletzia extends beneath the Willamette Valley and the old Cascades (Finn, 1990, Blakely, 1994, Trehu et al., 1994). The approximate location of its western edge is well-defined from seismic studies (e.g. Trehu et al., 1994, 1995; Hyndman et al., 1995) and magnetic anomaly maps (see figure 3a). This western limit lies beneath the continental shelf of central Oregon, beneath the coast in southwest Washington, and along the eastern edge of the Olympics in northwest Washington. Beneath Oregon, the Siletz terrane is at least 10 km thick offshore and 30 km thick under the Coast Range (Trehu et al., 1994). The

Figure 3a. NOAA shiptrack locations and magnetics along track, over National Geophysical Data Center (NGDC) 2D magnetics and bathymetry. Shiptrack location plot is zero axis to shiptrack magnetic data. Bathymetric contour interval is 100m above 500m depth, and 500m below. 200m contour is approximate location of shelf break. ST=Siletz terrane; 4=seafloor spreading anomaly 4, 4r=anomaly 4r, 4a=anomaly 4a (Wilson, 1993); HB=Heceta Bank; NB=Nehalem Bank. I, II, III interpreted to be due to an aseismic ridge (see text and Figure 11). NGDC data were found to be incorrectly located. By comparing gridded data to correctly located shiptrack data, we calculated and applied a small westward shift. NGDC data available from NOAA on Geophysics of North America CD-ROM, Release 1.0.

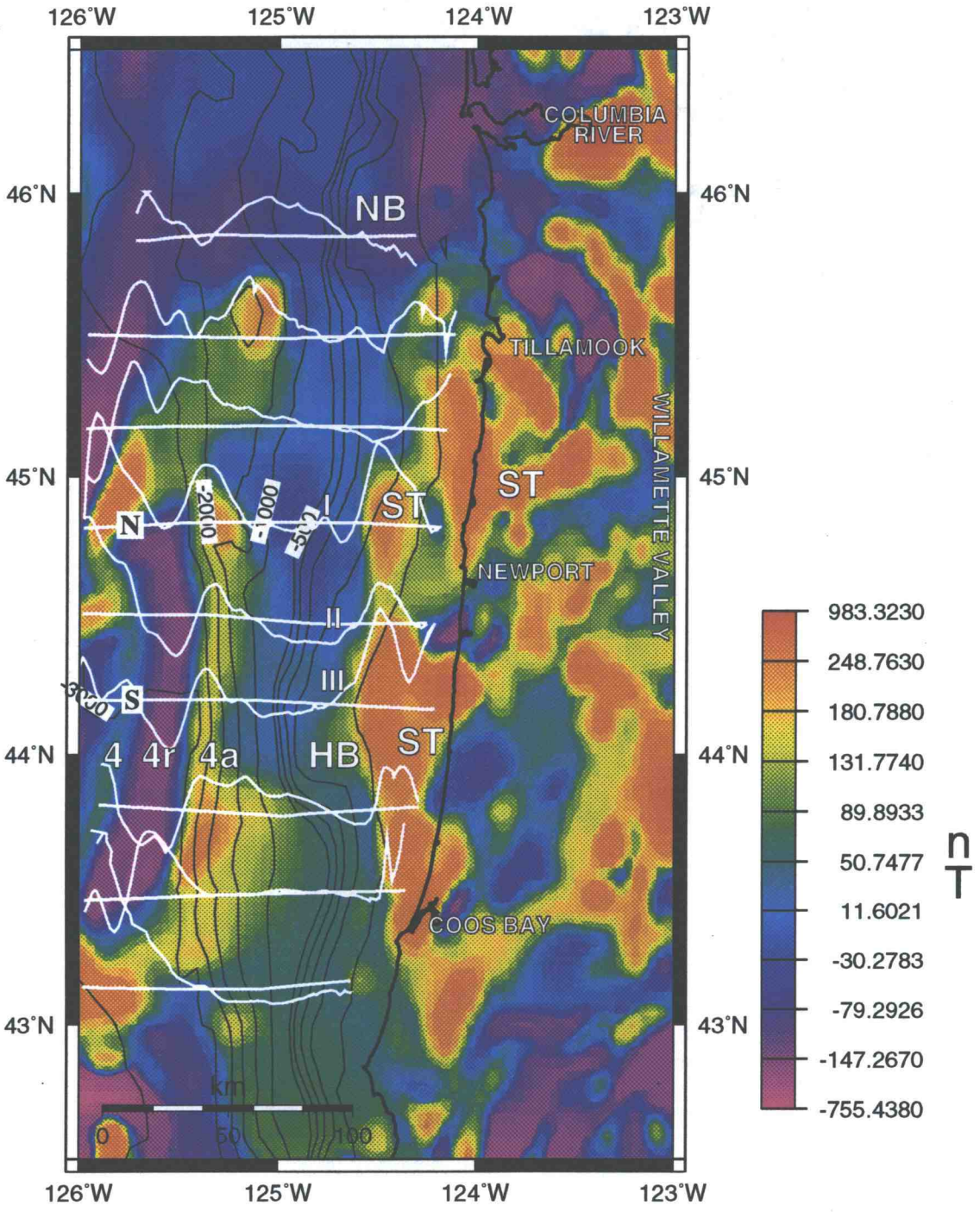
126°W
125°W
124°W
123°W
46°N
45°N
44°N
43°N
COLUMBIA RIVER
NB
TILLAMOOK
WILLAMETTE VALLEY
ST
ST
NEWPORT
N
S
I
II
III
4
4r
4a
HB
ST
COOS BAY
km
0
50
100
983.3230
248.7630
180.7880
131.7740
89.8933
50.7477
11.6021
-30.2783
-79.2926
-147.2670
-755.4380
nT

Figure 3a

Figure 3b. NOAA shiptrack locations and free-air gravity along track, over NGDC 2D gravity and bathymetry. NGDC gravity is free-air offshore, Bouguer onshore. Shiptrack location plot is zero axis to shiptrack gravity data. Bathymetric contour interval is 100m above 500m depth, and 500m below. 200m contour is approximate location of shelf break. ST=Siletz terrane; HB=Heceta Bank; NB=Nehalem Bank. NGDC data were found to be incorrectly located. By comparing gridded data to correctly located shiptrack data, we calculated and applied a small westward shift. NGDC data available from NOAA on Geophysics of North America CD-ROM, Release 1.0.

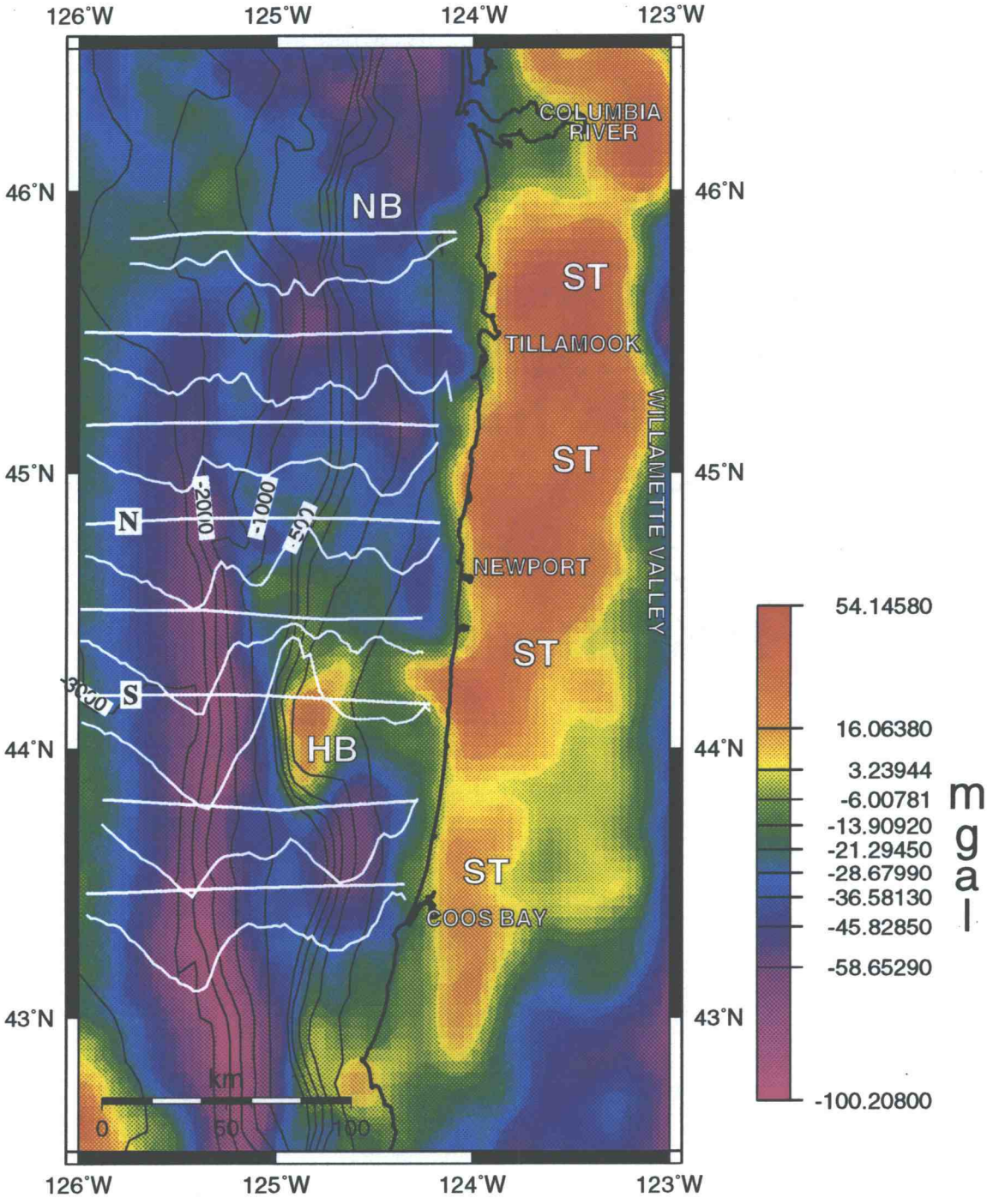
126°W
125°W
124°W
123°W
46°N
45°N
44°N
43°N
COLUMBIA RIVER
NB
ST
TILLAMOOK
WILLAMETTE VALLEY
ST
N
-2000
-1000
-500
NEWPORT
ST
S
-3000
HB
ST
COOS BAY
km
0
50
100
54.14580
16.06380
3.23944
-6.00781
-13.90920
-21.29450
-28.67990
-36.58130
-45.82850
-58.65290
-100.20800
mgal

Figure 3b

Siletz terrane thins significantly beneath northwest Oregon, continues to thin to the north, and has approximately the same thickness as normal oceanic crust where it is thrust beneath the pre-Tertiary terranes of Vancouver Island (Trehu et al., 1994, Hyndman, 1995).

The exposed rocks of the Siletz terrane are Paleocene to Eocene tholeiitic submarine pillow lavas and breccias which grade locally into subaerially erupted alkalic basalts (Snavely, 1968, Simpson and Cox, 1977, Duncan, 1982). These rocks were erupted at a number of local volcanic centres with K-Ar and ^{40}Ar-^{39}Ar ages decreasing from the north and south toward the Washington-Oregon border (Duncan, 1982). The basalts are interfingered with terrestrially-derived sandstones (Cady, 1975, Snavely, 1987), indicating formation close to shore. The geochemistry, stratigraphy, and age distribution of Siletz rocks suggest that the terrane may have formed at a spreading ridge (Duncan, 1982), a leaky transform resulting from plate reorganizations (Wells et al., 1984), or a short margin-normal rift resulting from oblique subduction (Wells et al., 1984). The great thickness of this terrane, which is similar to that of the Ontong Java plateau and other large igneous provinces (LIPs; see Coffin and Eldholm, 1993), suggests an anomalously rich magmatic source which may reflect the influence of the ancestral Yellowstone hotspot on one of the above mechanisms (Duncan, 1982; Trehu et al., 1994).

Stratigraphic evidence indicates that Siletzia was sutured to the North American continent by middle Eocene time. At its southern boundary, the early middle Eocene

Tyee formation overlaps the Siletzia/continental margin contact, indicating suturing by 50 Ma (Wells et al., 1984, Snavely, 1987). At the northern edge, dikes related to Cascade volcanism intrude Siletz basalts and indicate suturing by 42 Ma (Wells et al., 1984). Cloos (1993) calculated that an oceanic plateau on a subducting plate must be at least 100 km long by 50 km wide with a crustal thickness of ~30 km in order to block a subduction zone; the plateau would then be accreted to the continental margin and the subduction zone would move seaward of the accreted terrane, following the buoyancy model of Kelleher and McCann (1976). The subduction zone in the Pacific Northwest jumped from the extinct Challis volcanic arc in Idaho to the Cascade arc between 44 Ma and 35 Ma (Wells et al., 1984). Given the timing of these events and the size and nature of Siletzia, it is possible that the Siletz microplate jammed the subduction zone, causing it to jump westward to its current position (Simpson and Cox, 1977). A decrease in the Farallon-North America convergence rate between 43 Ma and 28 Ma may also be related to arc migration as either cause (Wells et al., 1984) or effect.

Changes in paleomagnetic rotations correlate well with changes in thickness of the Siletz terrane and crustal seismicity patterns. All basement rocks in the Oregon and Washington forearc have rotated clockwise (Simpson and Cox, 1977). In Washington, the Siletz terrane is broken into a number of smaller, independently rotating, fault-bounded blocks (Wells and Heller, 1988, Wells and Coe, 1985), but it behaves as a single, coherent block with a uniform rotation of ~70° in central Oregon (Magill et al., 1981). Most, if not all, rotation occurred post-accretion (Simpson and Cox, 1977,

Wells et al. 1984). Wells et al. (1988) propose that the rotation was due both to dextral shear between the NA and obliquely subducting Farallon plates and as a result of Basin and Range extension.

2.2 Morphology of the Oregon Continental Margin and Neotectonics

Active, potentially seismogenic, west-northwest-trending sinistral strike-slip faults have recently been identified in the Oregon accretionary prism (Goldfinger et al., 1992, in press; see figure 4). A number of topographic features on the Oregon continental margin are at least partially controlled by such structures (Goldfinger et al., in press). These faults appear to terminate over the seaward edge of the Siletz terrane as defined by magnetic maps, and drastically decrease in number in the Washington accretionary complex (Goldfinger et al., in press, McNeill et al., submitted), where the Siletz terrane is thinner and does not extend offshore. Movement on these faults may accommodate a significant amount of plate convergence (McCaffrey and Goldfinger, 1995, Goldfinger et al., 1992).

The seaward edge of the Siletz terrane in central Oregon also marks the position of a band of short-wavelength margin-parallel folds and faults that contrast sharply with larger-wavelength folds in the accretionary complex seaward of this point. Also, the Fulmar fault, a major N-trending dextral strike-slip fault hypothesized to have truncated the Siletz terrane in the late Eocene, appears to have been reactivated, as indicated by disruption of younger sedimentary strata over the western edge of the Siletz terrane imaged in MCS reflection data (Snavely et al., 1980, Snavely et al.,

Figure 4. Simplified neotectonic map. WCF=Willapa Canyon Fault; WF=Wecoma Fault; DBF=Daisy Bank Fault; ACF=Alvin Canyon Fault; HSF=Heceta South Fault; CBF=Coos Basin Fault; TRF=Thompson Ridge Fault (from Goldfinger et al., in press). NBF=Nehalem Bank Fault (from Goldfinger et al., in press; Goldfinger, 1994; Chris Goldfinger, pers. com., 1996). FF=Fulmar Fault (Snavely, 1987). NS-trending thrusts and anticlines are ubiquitous throughout accretionary prism. HB=Heceta Bank; NB=Nehalem Bank. Relative JdF/NA plate direction and velocity from Riddihough, 1984. Directions of maximum horizontal compressive stress given by large, unfilled arrows (from Werner et al., 1991; Zoback, 1992). Heavy dashed line gives approximate western limit of Siletz terrane as inferred from magnetic anomaly maps. Small crosses indicate axis of linear, continuous magnetic anomaly tentatively interpreted to be due to an aseismic ridge (see text and figure 11).

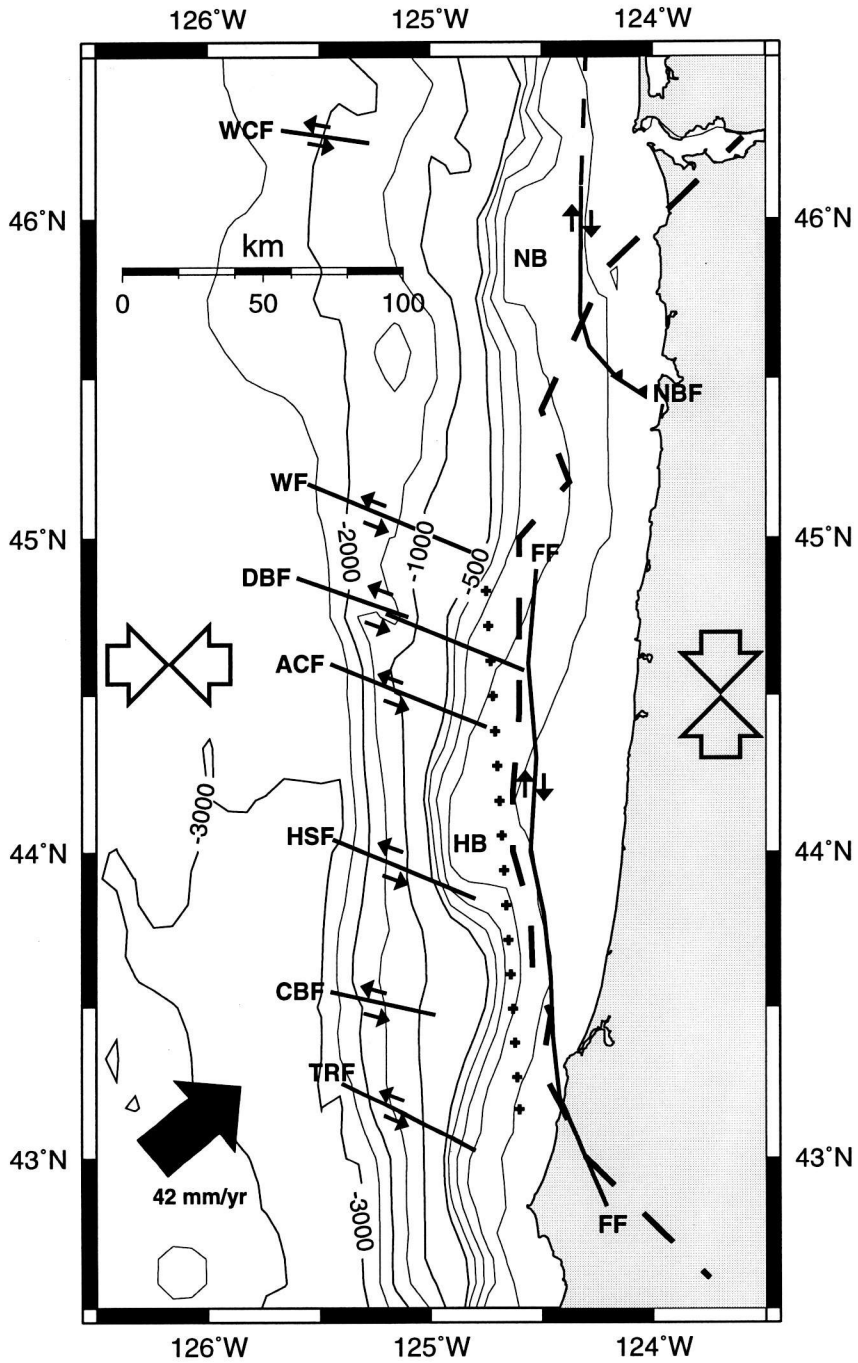
126°W
125°W
124°W
46°N
45°N
44°N
43°N
WCF
km
0
50
100
NB
NBF
WF
DBF
ACF
FF
HSF
HB
CBF
TRF
-500
-1000
-2000
-3000
42 mm/yr

Figure 4

Figure 5. Migrated MCS reflection line of Trehu et al. (1995). Thick black line at a 2-way travel time of ~2 to 3.3 s is top of block-faulted continental basement. Thick black line at ~0.4 to 1.7 s is a Neogene unconformity. Thick vertical lines at ~120 km denote the Fulmar fault. S and DB are thin Miocene basalts. Well is P-0103, T.D.=3849 m; synthetic seismogram from Cranswick and Piper (1991). Synthetic seismogram matches well with this dataset and coincident USGS and proprietary industry MCS reflection data. Interpretations of well logs (Snavely et al., 1980; Peterson et al., 1984; Snavely et al., 1987) support our seismic interpretation. Note diffractions at basement depths to left (west) of interpreted continental basement; a black dot denotes the apex of one such diffraction pattern. Distance is given in distance along our potential field model of the north line (see figure 6).

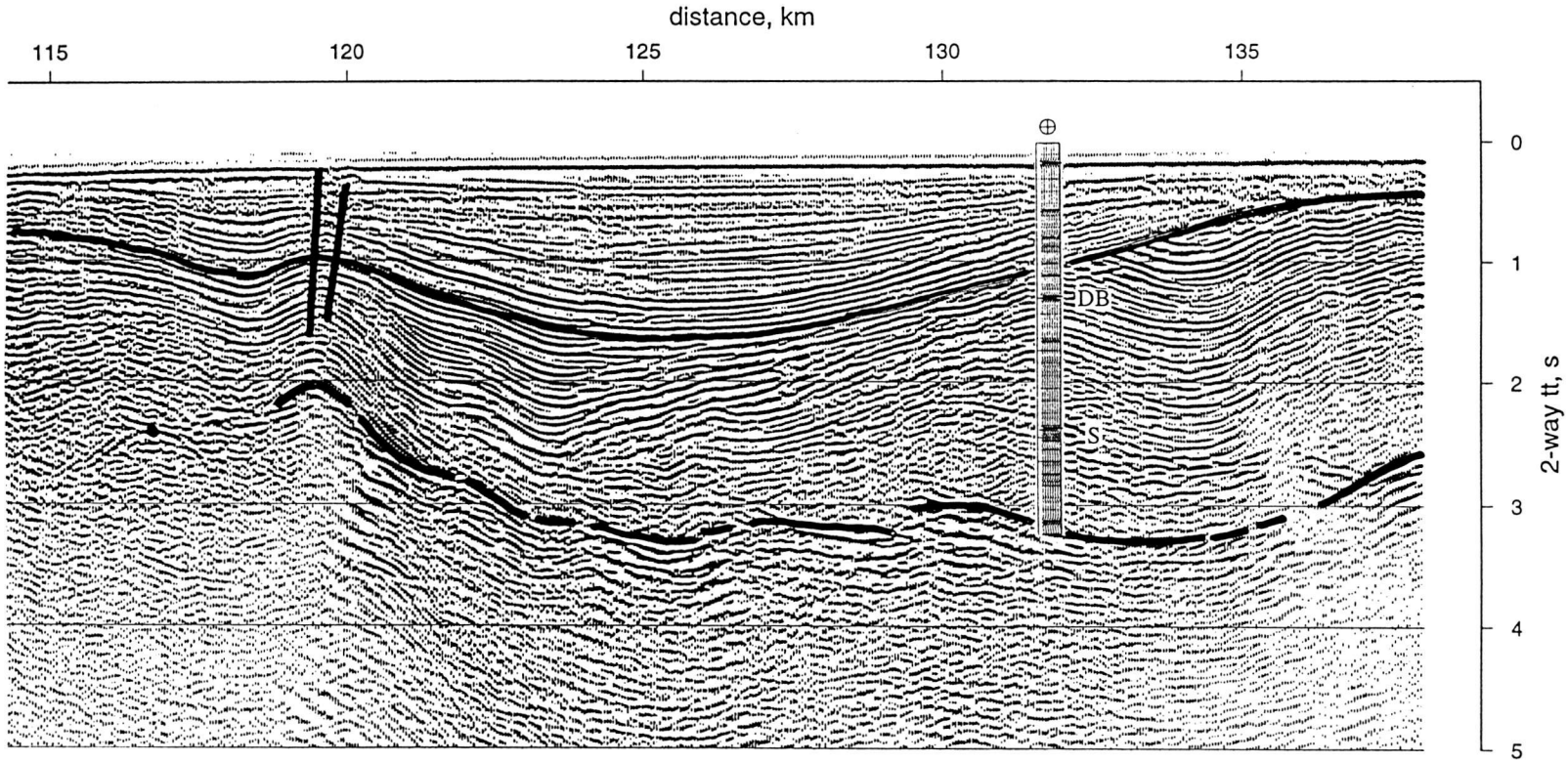

Figure 5

1985, Snavely, 1987; see figures 4 and 5). This deformation appears to extend to the seafloor in at least one place (Trehu et al., 1995; figure 5).

Heceta Bank is an enigmatic topographic feature located at approximately 44°00'N to 44°30'N and extending westward on the continental shelf to about 125°00'W. It is bounded to the south by active faults (Goldfinger et al., in press), and the short-wavelength folds lying over the apparent seaward edge of Siletzia are particularly prominent here (Charles Hutto, pers. com., 1996). The free-air gravity map clearly reflects its presence (figure 3b), but the simple spatial correlation between gravitational and bathymetric anomalies that would be expected if the gravity field reflected only topography and large-scale plate geometry is not observed (see figure 3b). Examination of 2D magnetic data suggest that the Siletz basement does not extend sufficiently far west to core Heceta Bank (compare figures 3a and 3b). Heceta Bank is interpreted to be at least in part the product of structural uplift due to underthrusting of young sediments at the bottom of the accretionary complex (Kulm and Fowler, 1974). However, existing data shed little light on the deep structure of the bank and the origin of the large observed gravity anomaly, and do not explain the margin-parallel variation in the width of the continental shelf.

3. POTENTIAL FIELD DATA

Marine magnetics and free-air gravity data along the continental margin from 43°00'N to 46°00'N were acquired independently by a number of agencies and universities and are available from the NOAA (National Oceanographic and Atmospheric Administration) Marine Trackline Geophysics database, available on CD-ROM. Data collected on different cruises were examined and found to be mutually consistent. Shiptrack data acquired by NOAA were selected for the modelling procedure because magnetics, gravity, and bathymetry were simultaneously collected, the shiptracks were oriented approximately perpendicular to the predominant N-S geological strike at the continental margin, and the survey lines were of the greatest spatial density and latest vintage. The data were resampled using an Akima spline with a 0.5 km sampling interval prior to modelling.

The large magnetic and gravity high running along the coastline, marked ST in figures 3a and 3b, corresponds to the Siletz terrane. The peak in the gravity anomaly is controlled by uplifted Siletz rocks exposed in the Oregon Coast Range, and the edges of the anomaly are affected by the presence of sedimentary basins in the continental shelf and Willamette Valley (figure 3b). The magnetic anomaly map closely mirrors the distribution of Siletz outcrops onshore, and clearly locates the seaward edge of crystalline basement offshore where it is juxtaposed against the accretionary complex (figure 3a). Changes in the gradient of the edge anomaly suggest variation in the shape of this boundary.

The N-S trending linear magnetic highs on the JdF plate, marked 4, 4r, and 4a on figure 3a, are seafloor magnetic lineaments. A magnetic quiet zone lies between the easternmost seafloor spreading anomaly and the Siletz anomaly. The nature of the low-amplitude, intermediate-wavelength magnetic anomalies lying in this quiet zone is not obvious and will be discussed in a later chapter. The smooth eastward decrease in the gravity field in the western half of the map reflects increasing depth to the dense, subducting JdF crust. This gravity low over the sediment-filled trough is characteristic of most subduction zones (Hyndman, 1995). Free-air gravity data between the coast and the abyssal plain reflect a complex interplay between seafloor topography, changing depth to the JdF plate, the internal density structure of the accretionary prism, the edge of crystalline continental basement, and the distribution of a number of small, shallow basins filled with unconsolidated sediments. The southern line very clearly reflects the presence of Heceta Bank (marked HB on figures 3a and 3b).

4. MODELLING

We used the GM-SYS gravity and magnetics modelling software of Northwest Geophysical Associates (Corvallis, OR). This application incorporates USGS SAKI code for performing least-squares inversion for selected model parameters (Webring, 1985). A summary of the mathematical techniques used in the software is given in the appendix. As the large-scale geometry of the Oregon continental margin consistently strikes N-S, perpendicular to the survey lines, and as small-scale variation is poorly constrained, our modeling procedure was restricted to 2D. The application supports both forward and inverse modelling of model body geometries, densities, and magnetic susceptibilities. Because of multiple trade-offs among various parameters, multiple starting models were considered and a hybrid forward/inverse approach was adopted, in which only a single parameter was varied at a time.

4.1 North Line, 44°48'N

A relatively large number of external geologic and geophysical constraints are available at the latitude of this profile. These include the refraction/reflection line of Trehu et al. (1994, 1995), USGS MCS reflection line L376W005 (Snavely, 1987), proprietary industry MCS reflection lines, and the cross-section of Snavely et al. (1980).

4.1.1 Model Geometry

The general geometry for the Siletz terrane, JdF plate, shelf sediments, and accretionary prism, including several relatively small, shallow basins, determined by Trehu et al. (1994) and illustrated in figure 2, was used in our potential field model. The model was extended in a laterally homogenous manner to ± 30,000 km in all horizontal directions to eliminate edge effects. Detail of the top of the Siletz terrane was interpreted from USGS MCS reflection line L376W005, a proprietary industry MCS reflection line, and the MCS line of Trehu et al. (1995) (figure 5) and converted to depth using a velocity of 1.8 km/s for unconsolidated Quaternary sediments and 3.0 km/s for compacted sediments lying between the Quaternary/Tertiary unconformity and the top of crystalline/seismic basement. Interpretations of well log data (Peterson et al., 1984) and a synthetic seismogram computed from the sonic logs (Cranswick and Piper, 1991) of an industry well (Well P-0103; T.D. = 3849 m.) (figure 5) generally confirm our interpretation of the seismic reflection data and our velocity estimates. The top surface of the Siletz terrane is imaged offshore in these datasets as a block-faulted reflector to model km ~118 in Figure 5 (Trehu et al., 1995). West of this location, several discontinuous diffractions are observed (figure 5), and basement can not be identified. Reflection, refraction, and OBS data indicate that the western limit of the Siletz terrane occurs near this location and that the Siletz edge dips steeply (Trehu et al., 1994; see figure 2). Two strong reflections, located at about 1.25 s and 2.4 s in the vicinity of the well, are observed in the data (DB and S, respectively, in figure 5). Drilling suggests these are Miocene basalts associated with the Depoe Bay and Cape Foulweather basalts onshore (Cranswick and Piper, 1993, Peterson et al.,

1984, Snavely et al., 1980). The spatial distribution of these basalts is not well-constrained, but the MCS data strongly suggest that they terminate at least 10 to 15 km east of the Siletz terrane's western edge and drilling shows the units to be thin (Snavely et al., 1980, Snavely, 1987, Peterson et al., 1984). These Miocene basalts were not included in the model.

4.1.2 Model Parameterization

All the significantly magnetic rocks in the region of study are basalts, which typically show remnant magnetization intensities equal to or greater than induced magnetization intensities (Koenigsberger ratio ≥ 1), so the magnitude and direction of remnant magnetization must be included in the model. For the JdF plate, starting values were a remnant magnetization intensity (the magnitude of the remnant magnetization vector), $|\mathbf{M_R}|$, of ± 0.001 emu/cm^3 (in general agreement with Finn, 1990 and Butler, 1992; plus and minus signs indicate normal or reversed polarity, respectively; bold font denotes a vector quantity) and a susceptibility, K, of 0.003 cgs units (in general agreement with Telford et al., 1990), found by forward modelling to yield a Koenigsberger ratio of ~1. Inclination, I, and declination, D, of the remnant field were set equal to that of the present geomagnetic field on the assumption that no major crustal rotations of the young JdF plate have occurred in the study area (Finn, 1990). From Wilson (1993), the positive seafloor spreading anomalies of figure 3a are anomalies 4 (~7.4 Ma) and 4a (~9.1 Ma), respectively. We calculated a half-spreading rate of 3.65 cm/yr over the 4 to 4a interval using Wilson's magnetic lineament map (1993) and the geomagnetic time scale of Cande and Kent (1992). A geographic

distribution of magnetic polarity within the JdF crust was determined from this rate and time scale, and was inserted into our model of the JdF plate.

Bromery and Snavely (1964) measured K = 0.0002 to 0.00625 cgs units for hand samples of the Siletz River Volcanics in Oregon. Finn (1990) directly measured a total magnetization intensity, $|\mathbf{M}|$, of 0.00275 emu/cm^3 for Crescent basalts in Washington. Her determination of remnant field direction is unusable as Siletz rocks in Washington have a separate rotation history from the Siletz block in Oregon, but Simpson and Cox (1977) measured an average D and I of 65.25° and 58.5°, respectively, for Siletz River Volcanics in our study area. However, the Siletz basalts may have been emplaced over a time frame including more than a dozen geomagnetic reversals (Fowler, 1990, Cande and Kent, 1992) and are interbedded with nonmagnetic sedimentary rocks. The internal stratigraphy of the offshore portion of the Siletz terrane we model here is unknown. Thus, Siletzia consists of an unconstrained vertical and horizontal distribution of normal and reverse magnetization polarities and finite and zero $|\mathbf{M_R}|$ and K.

In order to parameterize such a model, it is useful to briefly consider the physics of the problem. In general, the expression for the magnetic field vector $\mathbf{F}(\mathbf{r_o})$ at a distance $|\mathbf{r_o}-\mathbf{r}|$ from a magnetic body with arbitrary three dimensional geometry, v, and total magnetization vector $\mathbf{M}(\mathbf{r})$, is:

$$\mathbf{F}(\mathbf{r}_o) = \text{grad} \int_V \mathbf{M}(\mathbf{r}) \cdot \text{grad} \, (|\mathbf{r}_o - \mathbf{r}|)^{-1} \, dv \qquad \text{(Telford et al., 1990, p.66)} \qquad (1)$$

where $\mathbf{r}$ denotes the position vector of a point within the magnetic body and $\mathbf{r}_o$ denotes the position vector of an observation point outside the body.

The measured field $\mathbf{F}_T(\mathbf{r}_o)$at a position $\mathbf{r}_o$ on the earth's surface is, by superposition,

$$\mathbf{F}_T(\mathbf{r}_o) = \mathbf{F}_E(\mathbf{r}_o) + \mathbf{F}_I(\mathbf{r}_o) + \mathbf{F}_R(\mathbf{r}_o) \qquad \text{(ibid, p.66)} \qquad (2)$$

where $\mathbf{F}_E(\mathbf{r}_o)$ is the ambient geomagnetic field and $\mathbf{F}_I(\mathbf{r}_o)$ and $\mathbf{F}_R(\mathbf{r}_o)$ are the induced and remnant fields, respectively, due to some buried magnetic body. The ambient geomagnetic field is assumed to be a known constant within our study area. From (1), the induced and remnant fields are:

$$\mathbf{F}_I(\mathbf{r}_o) = \text{grad} \int_V \mathbf{M}_I(\mathbf{r}) \cdot \text{grad} \, (|\mathbf{r}_o - \mathbf{r}|)^{-1} \, dv \qquad (3)$$

where $\mathbf{M}_I(\mathbf{r})$ = induced magnetization vector = $\mathbf{K}(\mathbf{r})\mathbf{F}_E(\mathbf{r})$ (ibid, p.92), and:

$$\mathbf{F}_R(\mathbf{r}_o) = \text{grad} \int_V [\mathbf{M}_R(\mathbf{r}) \cdot \text{grad} \, (|\mathbf{r}_o - \mathbf{r}|)^{-1} \, dv] \qquad (4)$$

where $\mathbf{M_R(r)}$ = remnant magnetization vector. The magnitude of this vector is the remnant magnetization intensity, $|\mathbf{M_R(r)}|$, and its direction is conventionally described by the inclination, I(**r**), and declination, D(**r**).

So, for a given point of observation, $\mathbf{r_o}$, and magnetic body geometry, v,

$$\mathbf{F_T(r_o)} = f\,[K(\mathbf{r}),\ |\mathbf{M_R(r)}|,\ D(\mathbf{r}),\ I(\mathbf{r})]$$

What is known about these parameters? D and I determined by Simpson and Cox (1977) for 33 samples of Siletz River Volcanics, from different locations and representing a variety of ages, exhibit a narrow range of values within a 95% confidence interval. The remnant field in these rocks appears to flip back and forth by 180° with little wander. Also, the Siletz terrane of central Oregon is widely interpreted to have rotated post-formation, so rotation is uniform down-section, and as a single block, so rotation is uniform throughout the study area. As a result, if polarity reversals are represented as changes in the sign of $|\mathbf{M_R}|$, then D and I are not a function of position and the Siletz terrane may be modelled, in terms of remnant field direction, as a homogenous body with Simpson and Cox's (1977) measured values of D and I.

As previously noted, we have a measure of K and of the absolute value of $|\mathbf{M_R}|$ but not of the horizontal and vertical distributions of reversals, nonmagnetic sedimentary rocks, or variations in the magnitudes of K and $|\mathbf{M_r}|$. The lack of high-

amplitude, short-wavelength features in the magnetic signature of the offshore portion of Siletzia in both magnetic maps and shiptrack magnetics, and the absence of clear variation in the magnetic signature of the onshore portion of Siletzia not attributable to outcrop patterns, strongly suggest that variations in magnetic properties are distributed on a much smaller length scale than the crustal scale of the Siletz terrane itself. We therefore adopt a single bulk value for the remnant magnetization intensity and susceptibility for Siletzia as a whole, which represents the net superposition of the remnant and induced fields, respectively, of many smaller pockets of variously magnetized rock. As magnetic properties typically vary by orders of magnitude in a single outcrop (Shaul Levi, pers. com., 1996), our approach is simply an application to crustal scales of a simplification implicitly made in any magnetic modelling effort.

To assign a single value to this bulk measure of $|\mathbf{M}_R|$, we consider the paleomagnetic data of Simpson and Cox (1977) and the geomagnetic reversal scale of Cande and Kent (1992) and note that the number of normally magnetized samples and the proportion of time the geomagnetic field spent in a normally magnetized state over the course of formation of Siletzia, respectively, are comparable to their reversely magnetized counterparts. Note also that as D and I are approximately constant throughout the Siletz terrane, the remnant field directions of normally and reversely magnetized pockets within the terrane are approximately parallel or antiparallel. Clearly then, superposition of the magnetic signatures of normally and reversely magnetized pockets leads to destructive interference, so that when considered at a crustal scale, the absolute value of the bulk $|\mathbf{M}_R|$ will be very much less than that of

any one quasi-uniformly magnetized pocket. We thus make the simplifying assumption that bulk $|\mathbf{M_R}|$ for the Siletz terrane is zero. The magnetic response of the Siletz terrane is attributed entirely to induced magnetization, an assumption normally reserved for magnetic studies of non-basalt provinces. The observation that the Siletz terrane produces a strong positive magnetic anomaly over the entire region of study, in spite of the fact that volumetrically about half of it consists of reversely magnetized rock, provides strong additional evidence that net $\mathbf{F_R} <<$ net $\mathbf{F_I}$, so $|\mathbf{M_R}|$ may be neglected. The process of assigning a number to bulk susceptibility involves inverse modelling and is described later in this paper.

Densities for our initial model were determined by calculating a best-fit polynomial to the well-known Nafe-Drake velocity vs. density data and applying it to the gridded velocity model developed from the refraction/OBS work of Trehu et al. (1994). The resulting gridded density model was then used as a guide to assigning starting densities to the discretized model geometry described at the beginning of this section. Densities thus determined are in general agreement with Telford et al. (1990), Finn (1990), and Godfrey et al. (in press).

4.1.3 Modelling Results

Our current working model of the Oregon convergent margin at 44°48'N, based on modelling of magnetics and gravity data and the previously described external geological and geophysical constraints and assumptions, is given in figure 6. Density, K, $|\mathbf{M_R}|$, D, and I of each body in the model are given in table 1.

Figure 6. Potential field model of Oregon convergent margin at 44°48'N (north line). Model parameters are given in Table 1. Body 1: water; bodies 2, 4-6: accretionary complex; 3: oceanic sediments; 7-9: continental basement; 10: aseismic ridge; 11-34: JdF crust; 35: oceanic mantle. V.E. = 2

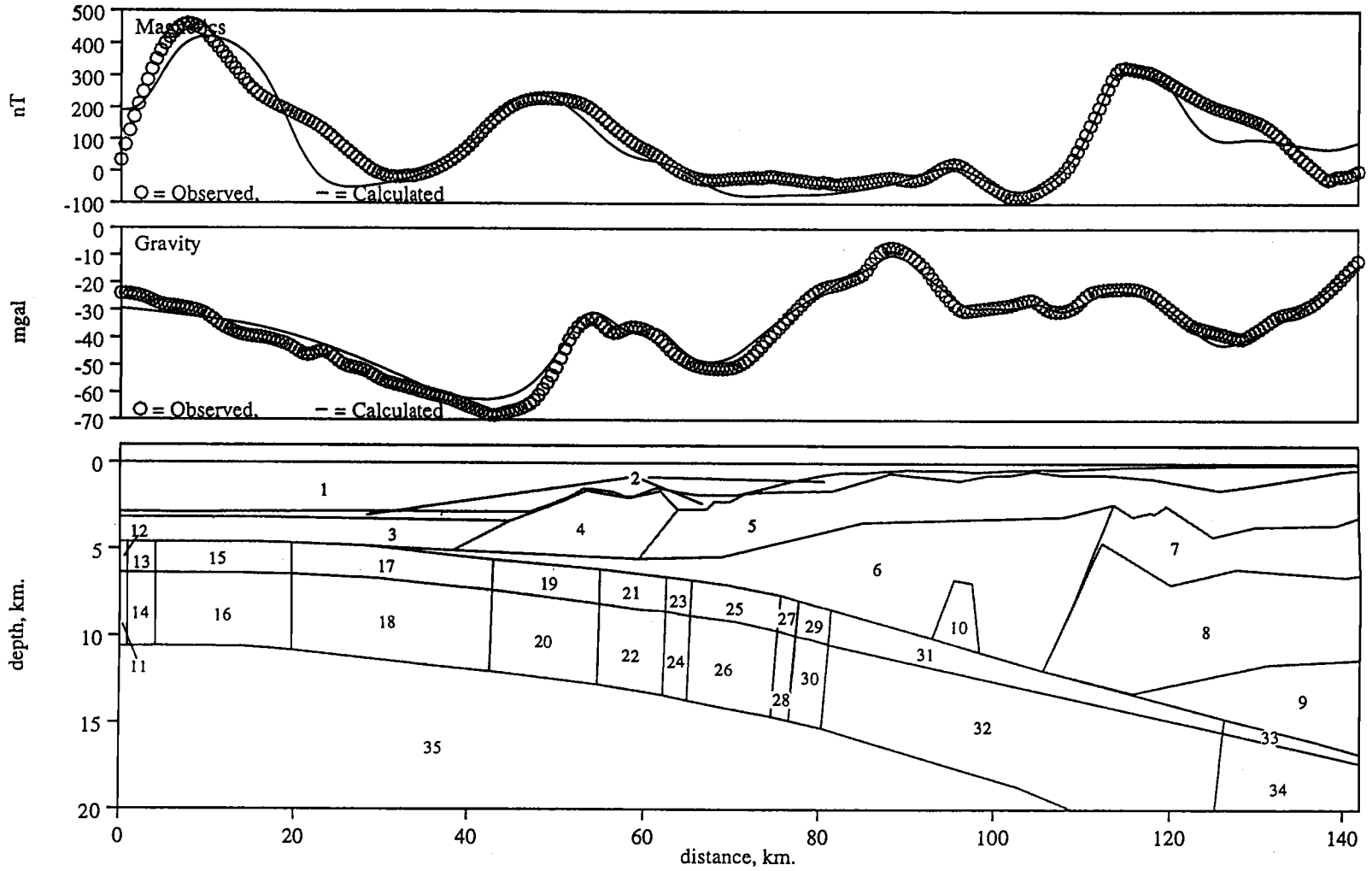
nT
Magnetics
O = Observed, – = Calculated
mgal
Gravity
O = Observed, – = Calculated
depth, km.
distance, km.

Figure 6

Body	Density (g/cc)	K (cgs units)	|Mr| (emu/cm3)	D (degrees)	I (degrees)	Geology
1	1.024	0	0	-	-	water
2	1.8	0	0	-	-	shallow basin fill
3	2	0	0	-	-	oceanic sediments
4	2.2	0	0	-	-	accretionary prism sediments
5	2.33	0	0	-	-	accretionary prism sediments
6	2.54	0	0	-	-	compacted prism sediments
7	2.65	0.00285	0	-	-	upper Siletz terrane
8	2.72	0.00285	0	-	-	middle Siletz terrane
9	3.1	0.00285	0	-	-	lower Siletz terrane
10	2.7	0.003	0.001	19	69	aseismic ridge
11	2.95	0.003	0.001	19	69	lower Juan de Fuca plate
12	2.65	0.003	0.001	19	69	upper Juan de Fuca plate
13	2.65	0.003	-0.001	19	69	upper Juan de Fuca plate
14	2.95	0.003	-0.001	19	69	lower Juan de Fuca plate
15	2.65	0.003	0.002	19	69	upper Juan de Fuca plate
16	2.95	0.003	0.002	19	69	lower Juan de Fuca plate
17	2.65	0.0035	-0.00075	19	69	upper Juan de Fuca plate
18	2.95	0.0035	-0.00075	19	69	lower Juan de Fuca plate
19	2.65	0.003	0.00125	19	69	upper Juan de Fuca plate
20	2.95	0.003	0.00125	19	69	lower Juan de Fuca plate
21	2.65	0.0032	-0.0005	19	69	upper Juan de Fuca plate
22	2.95	0.0032	-0.0005	19	69	lower Juan de Fuca plate
23	2.65	0.003	0.0012	19	69	upper Juan de Fuca plate
24	2.95	0.003	0.0012	19	69	lower Juan de Fuca plate
25	2.65	0.00275	-0.001	19	69	upper Juan de Fuca plate
26	2.95	0.00275	-0.001	19	69	lower Juan de Fuca plate
27	2.65	0.002	0.0008	19	69	upper Juan de Fuca plate
28	2.95	0.002	0.0008	19	69	lower Juan de Fuca plate
29	2.65	0.0015	-0.00075	19	69	upper Juan de Fuca plate
30	2.95	0.0015	-0.00075	19	69	lower Juan de Fuca plate
31	2.65	0.0008	0.0005	19	69	upper Juan de Fuca plate
32	2.95	0.0008	0.0005	19	69	lower Juan de Fuca plate
33	2.65	0	0	-	-	upper Juan de Fuca plate
34	2.95	0	0	-	-	lower Juan de Fuca plate
35	3.2	0	0	-	-	oceanic mantle

Table 1. Model parameters for north line (figure 6)

During preliminary modelling of the JdF plate alone, which was undertaken to better constrain the magnetic background to the Siletz edge signature, it was found that the observed magnetic quiet zone (see figure 3a) can not be attributed solely to deeper burial of the JdF plate. Using the initial values of $|M_R|$ and K for oceanic basalt and the spatial distribution of reversals described above, forward modeling of the JdF plate predicts a very long-wavelength anomaly with a peak-to-peak amplitude of about 180 nT in this quiet zone (figure 7). The geometry of the JdF plate is well-constrained, the calculated spatial distribution of reversals used in the model is based on well-known seafloor spreading anomalies to the west of the magnetic quiet zone, and our initial, nominal values of $|M_R|$ and K ($\pm$0.001 and 0.003, respectively) required only minor adjustment to match seafloor magnetic lineaments in the abyssal plain, suggesting that they are reasonable. The magnetically quiet character of this part of the trench must, therefore, reflect a decrease in the magnetic properties of the oceanic crust as it is being subducted rather than simple attenuation due to increased depth of burial. Our best-fit model of the JdF plate includes a progressive decrease in both susceptibility and in the absolute value of $|M_R|$ from values very similar to our starting values at anomaly 4a to less than half these values by about model km 85.

In spite of the fact that the Cascadia subduction zone is unusually hot due to the young age of the JdF plate and the insulating effects of thick sediment cover (Hyndman and Wang, 1993), subduction zones in general are low-temperature environments and thermal models of Cascadia (Hyndman and Wang, 1993, Oleskevich,1994) suggest that Curie temperatures of 550-600°C (Milsom, 1989, p.46)

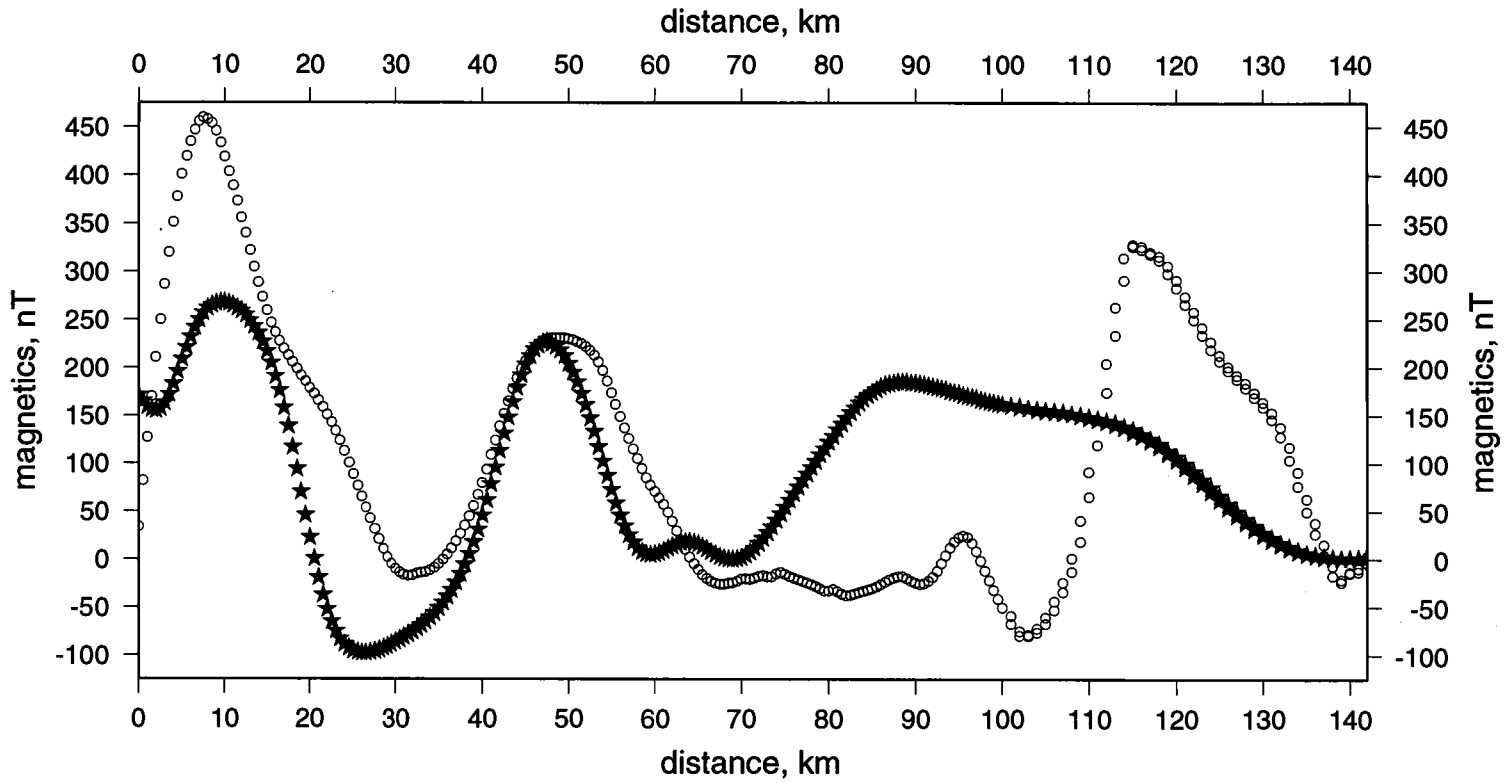

Figure 7. Magnetics along track, north line. Comparison of observed data (empty circles) with forward-modelled magnetic response (solid stars) of JdF plate only, with K=0.003 cgs units and $|M_i| = \pm 0.001$ emu/cm^3, using horizontal distribution of JdF reversals from Wilson (1993) and Cande and Kent (1992) as shown in Figure 6. Gradual eastward demagnetization of JdF crust required starting at ~70 km.

are not reached on the thrust plane until about 175-200 km east of the deformation front, beyond the extent of our magnetic model. However, Hyndman and Wang (1993) assume for their central Oregon model only a thin strip of Siletz basalt analogous to that observed in Vancouver Island, and Oleskevitch (1994) assumes an arcward dip to the Siletz edge and thus a smaller basalt volume than would result from a trenchward dip. Hyndman and Wang (1993) point out that a thicker Siletz terrane here would result in a model with higher thrust plane temperatures. Moreover, temperatures within the ~6 km thick JdF crust obviously increase with depth from the thrust plane temperatures calculated by these thermal models; it is thus possible that Curie temperatures are attained at some depth within the subducting JdF plate, reducing from the bottom up the volume of magnetic rock within the oceanic crust and resulting in a magnetic quiet zone. It is also possible that hydrothermal alteration of the subducting oceanic crust below the continental slope, consisting of metamorphism of basalts and recrystallization of iron-titanium oxides, could destroy the remnant magnetism of the rock (Scheidegger, 1984, Finn, 1990), significantly reducing its magnetic response. Stable oxygen isotopic analysis of carbonate cements in accreted sediments at the central Oregon deformation front indicate circulation of high-temperature fluids upwards from the decollement (Sample et al., 1993). Large volumes of fluid released from a subducting slab during prograde metamorphism of hydrated oceanic crust lead to trenchward advective heat transport by fluid flow channeled along the shear zone and exothermic retrograde reactions in the hanging wall of the shear zone (Peacock, 1987), conceivably leading to hydrothermal alteration and demagnetization of JdF basalts. The petrogenetic grid compiled by Cloos (1993)

suggests that for a comparatively warm subduction zone such as Cascadia, significant metamorphism may take place in the subducting slab at depths that are attained by the JdF plate in the observed magnetic quiet zone. The presence of turbidite-hosted mesothermal gold deposits within the Alaska accretionary prism illustrates that it is possible for very hot fluids to circulate through such a nominally low-temperature tectonic setting (Haeussler et al., 1995). Regardless of the origin of the progressive eastward demagnetization of JdF basalts in the magnetic quiet zone, the effect is real and is incorporated into our model.

Because magnetic modelling is most sensitive to the shorter-wavelength response of shallow structure (Webring, 1985), we were able to determine through trial-and-error that the upper surface of the Siletz terrane must extend slightly seaward and upward of the westernmost position it is imaged in seismic data. This conclusion was found to be highly insensitive to Siletzia bulk K. However, equation 1 shows that the modelled geometry of the edge of the Siletz terrane (information contained in v) and its modelled susceptibility (information contained in $\mathbf{M}(\mathbf{r})$) are theoretically interdependent (see also Webring, 1985). Consequently, evaluation of the sensitivity of modelled geometry to modelled susceptibility is necessary when considering the geometry of the entire backstop. Assuming that the western side of the Siletz terrane is a straight line in cross-section, we created 64 models, representing eight values of susceptibility and eight values of dip, holding all other model parameters constant. The RMS error for each model was used as a measure of the quality of fit of each of the forward-modeled magnetic responses to the observed data, and is plotted as a

function of dip and susceptibility on figure 8. The results illustrate the degree of sensitivity of dip angle to bulk susceptibility and delineate a range of acceptable values for both. Based on this analysis, the best fit dip and susceptibility are 55°W and 0.00285 cgs units (figure 9a).

We have thus far arbitrarily assumed that the western edge of Siletzia forms a straight line in cross-section. Figures 9b and 9c are examples of two other configurations that result in an equally good match to the magnetic data. Both consist of a westward dip of the upper backstop, with an arcward dip below; the model of figure 8c includes thrusted or offscraped JdF plate material underneath the leading edge of continental basement. The relationship between Siletz edge geometry and bulk Siletz K remains unchanged. It was found iteratively that significantly different geometries, including a vertical or eastward dip to the Siletz terrane edge for depths less than ~7 km, do not match the data, regardless of the susceptibility used. We conclude that magnetic modelling, in concert with existing geologic information and our initial assumptions, constrains the geometry of the seaward edge of the Siletz terrane at 44°48'N to a 45° to 55° westward dip to a depth of ~7 km. Below this depth, the geometry of the Siletz terrane remains poorly constrained, mostly due to the decreasing sensitivity of magnetic data with increasing depth.

The fit of our calculated magnetic anomaly to the observed data is poor around model km 140 (figure 6). Snavely et al. (1980) place two Miocene basalts at this position on the basis of an industry well (see also Peterson et al., 1984, Cranswick and

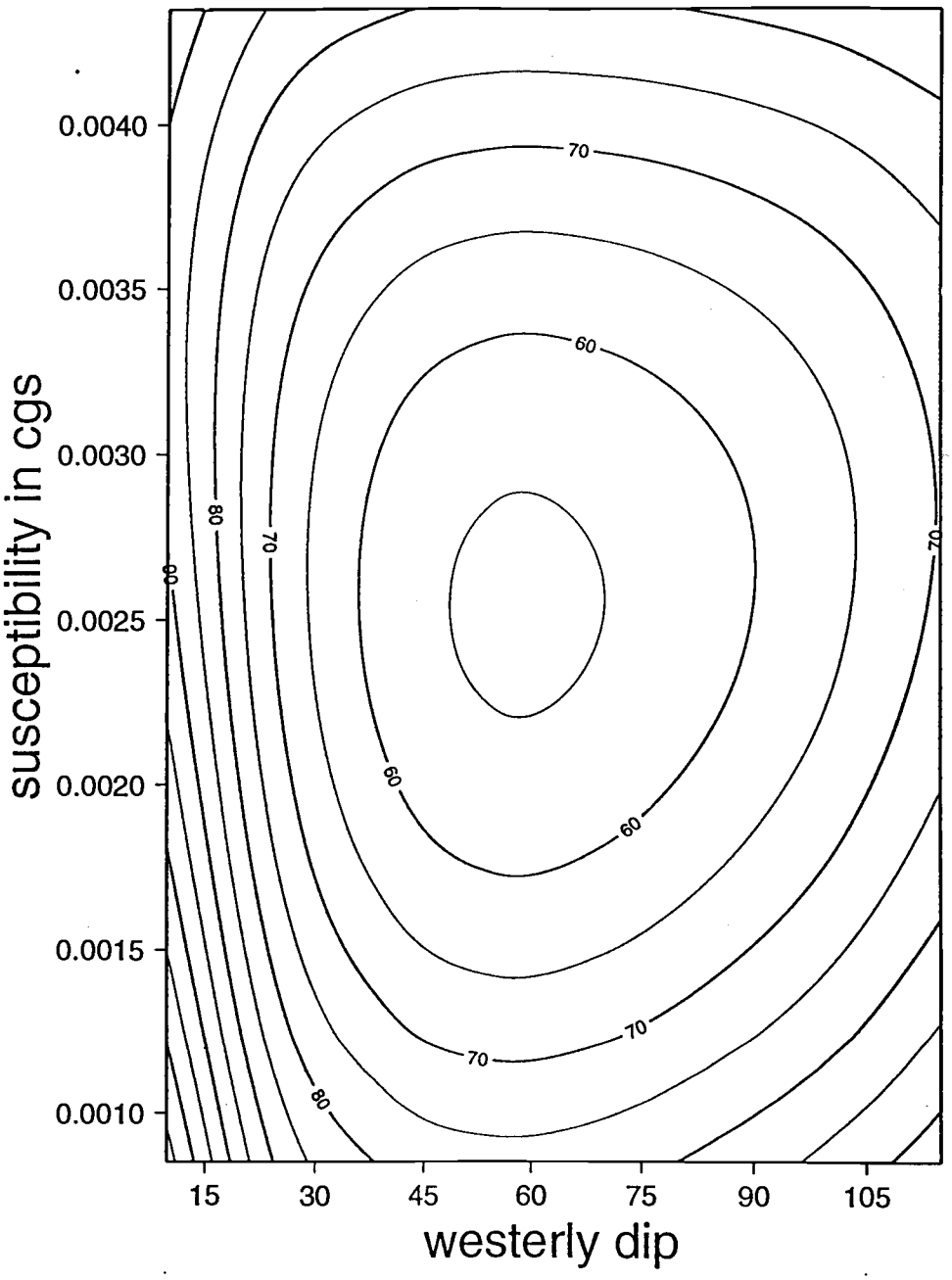

Figure 8. Contour plot of RMS error as a function of dip of the Siletz edge and bulk susceptibility of the Siletz terrane. 64 models were calculated, representing eight values of magnetic susceptibility bracketing our tentative model value of 0.00285 cgs units in 0.0005 steps, and eight values of dip bracketing our tentative model value of 55° W in 15° steps. All other model parameters were held constant. Backstop assumed to be a straight line in cross-section.

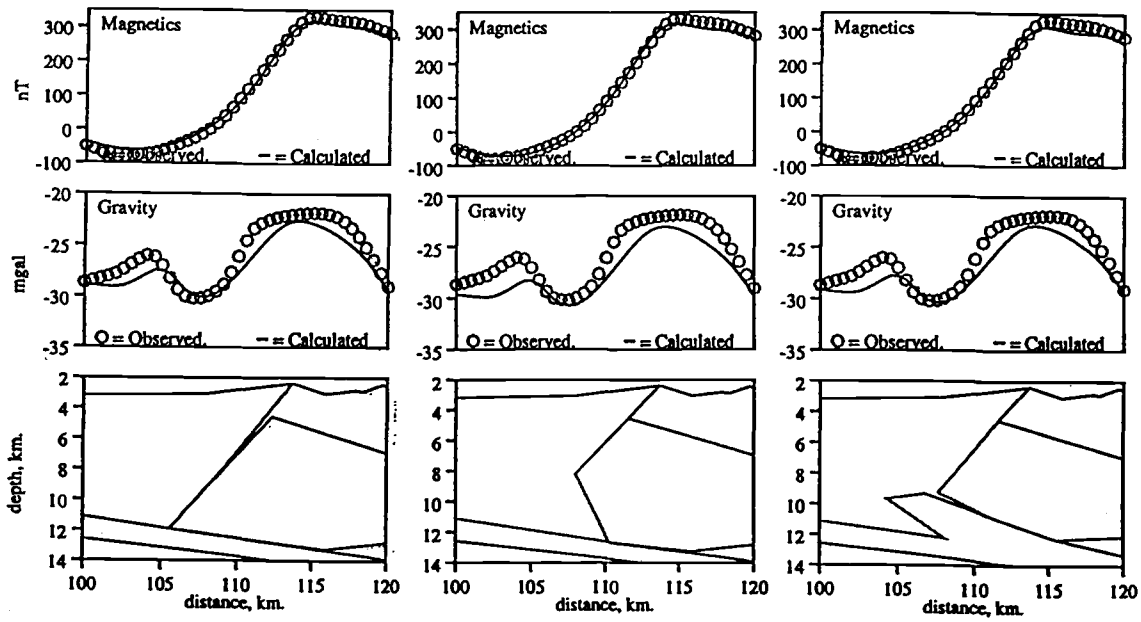

9.a) 9.b) 9.c)

Figure 9. Examples of acceptable backstop models, north line. 9.a) seaward-dipping to JdF plate (model of figure 6); 9.b) landward-dipping below ~8 km. depth; 9.c) landward-dipping below ~8 km. depth, floored by thrusted and/or underplated JdF crust. Model parameters identical in all cases to those of figure 6 and Table 1. V.E. = 1

Piper, 1993). MCS reflection data indicate that these basalts terminate by about model km 130 (Snavely et al., 1980) (figure 5). In addition, the industry well bottomed in what is interpreted to be a Yachats-equivalent middle to upper Eocene basalt (Snavely et al., 1980, Snavely, 1987). The upper Eocene basalt, which is younger than the Siletz terrane, closely corresponds in 2-way travel time to the seismic event we used to define continental basement (figure 5). However, reflection and refraction data clearly show this reflection to be the top of seismic basement. If it is indeed a Yachats-equivalent basalt, then there must be relatively little sediment separating the bottom of this formation from the top of the Siletz River volcanics. It must still represent acoustic and magnetic basement and the use of this reflection to map out the top of continental basement remains justified. However, these upper Eocene and Miocene basalts, which we have omitted from our model due to a lack of precise constraints on their extent and their lack of influence on models of the Siletz terrane edge, could account for the high-amplitude, relatively short-wavelength mismatch here if the body has a significant and predominantly reversed remnant magnetization. The small area of the corresponding 2D magnetic low (figure 3a) tends to confirm this interpretation.

For the gravity model, subdivision of the accretionary prism and Siletz terrane into several bodies generally increasing in density arcward and downward represents for the most part the discretization of continuous density gradients implied by the velocity model. The gravity data required some modification of densities from the initial values derived from the velocity model. This may be in part a result of the

discretization process but more strongly reflects uncertainty in the velocity model and in the rough approximation of density from seismic velocity. The densities in our final gravity model remain consistent with those predicted from the velocity model via the Nafe-Drake relationship (figure 10).

All three Siletzia geometries inferred from magnetic modelling (figure 9) are consistent with the gravity data. The free-air gravity data are relatively insensitive to the moderate density contrasts across the Siletzia/accretionary prism lateral contact, reflecting better the large density contrasts due to topography and shallow basins, as well as such large-scale features as the subducting JdF plate. These features are fairly well-constrained, so the gravity data is best suited to discerning mass distributions deeper within the thick accretionary complex.

The velocity model of Trehu et al. (1994) suggests relatively high sediment densities in the accretionary prism seaward of the backstop, starting at a depth of ~2.5 km and continuing down to the subducting oceanic crust (figure 2). The gravity data are consistent with this interpretation.

The velocity model also suggests a deep pocket of anomalously high velocity between model km 80-100 (figure 2). This is consistent with the gravity data, although there is a trade-off between the density and volume of this feature. To address the issue, we return to the magnetics data. At the approximate location of this mass concentration, there is a small-amplitude, medium-wavelength magnetic anomaly

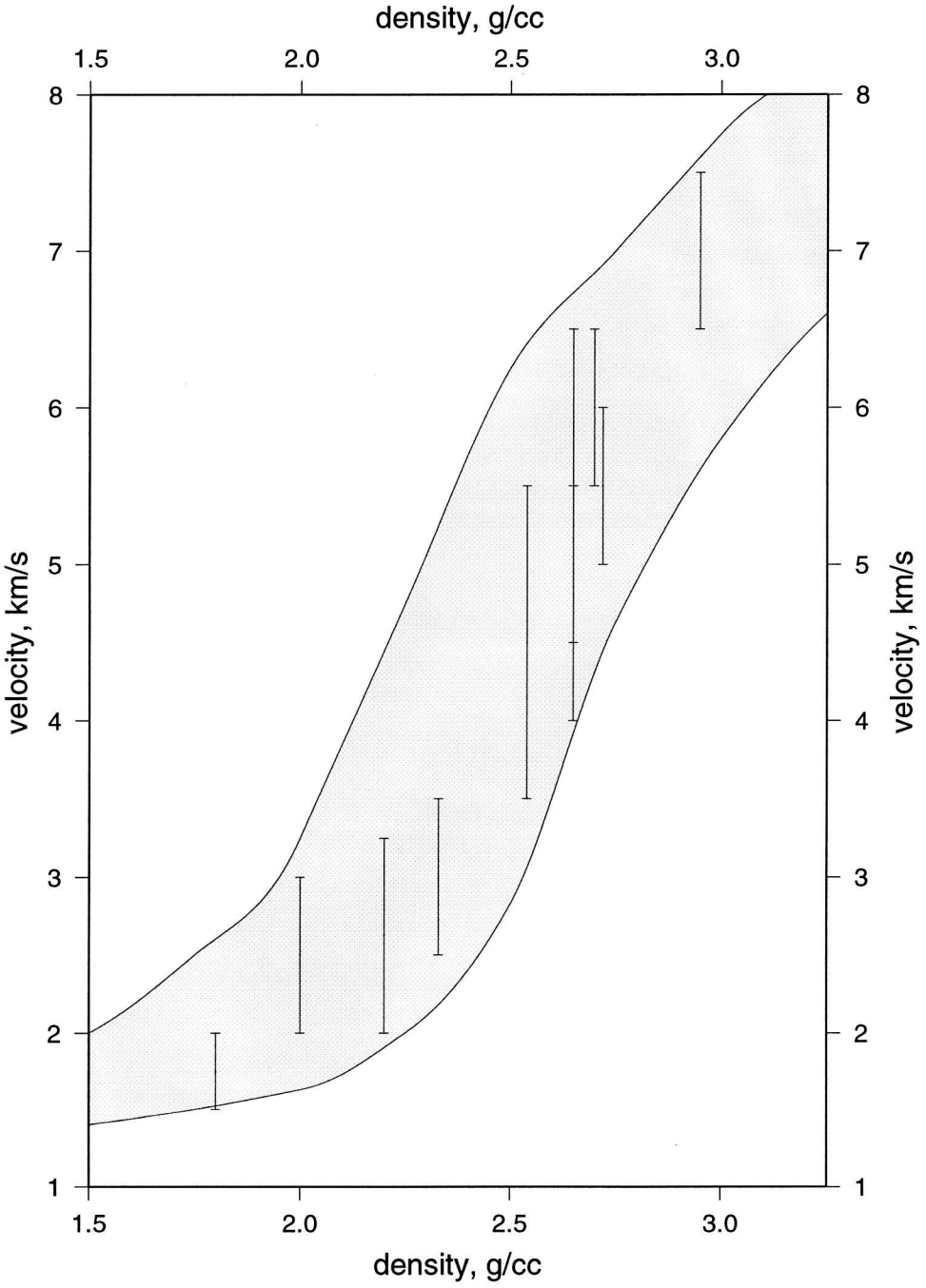

Figure 10. Plot of densities of discrete bodies in our potential field model of the north line (figure 6) against corresponding range of velocties (vertical bars on diagram) from nondiscretized velocity model (figure 2). Grey area is range of velocities permitted by Nafe-Drake data for a given density (Fowler, 1990). Our final gravity model remains consistent with the original velocity model.

(marked I on figure 3a) within the magnetic quiet zone. This anomaly appears to be traceable to the central and south NOAA lines, and is marked II and III, respectively, on figure 3a. Figure 11 is a perspective plot of the magnetic anomaly data, illuminated from the west and viewed from the southwest. The N- to slightly NNW-trending anomaly is linear and continuous from 45°00'N to about 42°00'N. At its southern limit (~42°00'N to ~43°00'N), several positive anomalies are clearly present as conical features in figure 11 and and as "bull's eyes" in figure 3a. These are suggestive of seamounts lying on the JdF plate, buried beneath the continental shelf (Tom Brocher, pers. com., 1996). Seafloor spreading anomalies are disrupted between roughly 126°00'W, 43°15'N and 125°10'W, 43°40'N (figure 3a). Interpretations of spreading anomalies (e.g. Wilson, 1993) suggest this is due to a pseudofault which separates the JdF spreading anomalies in this region into two distinct zones. This feature can not be traced west to the linear magnetic anomaly under consideration due to the intervening magnetic quiet zone, but a rough linear projection places the intersection of the pseudofault with the coastline just south of Heceta Bank. The linear anomaly thus crosses this discontinuity in the JdF plate. The linear anomaly is parallel to the spreading anomalies north of the inferred pseudofault, and appears to be oblique to the spreading anomalies to the south of the discontinuity, which are rotated clockwise relative to their counterparts to the north.

The linear anomaly can not be modelled as a seafloor magnetic lineament because its wavelength is too short to be produced by a source at the depth of the subducting crust, and because it crosscuts the pseudofault. It can not be modelled as an abyssal

Figure 11. 3D plot of NGDC magnetic data in narrow N-S strip along Oregon convergent margin, illuminated from W, viewed from SW. Large, ~N-S trending anomaly in eastern half of data is Siletz response (see figures 3a, 6). Thick Siletz basalts turn inland at ~43°N and ~45°30'N. Small-amplitude, medium-wavelength, linear, and ~continuous N- to NNW-trending anomaly (I, II, and III of figure 3a; model km 90-100, figure 6; model km 100-110, figure 12), immediately to the west of the Siletz anomaly, is tentatively interpreted to be the magnetic response of an aseismic ridge. At the latitude of Heceta Bank (~43.8°N to ~44.4°N), this anomaly partially merges with the Siletz anomaly, suggesting close proximity or collision of the inferred ridge with the backstop. Conical anomalies around 42° to 42°30', and a little north of 43°, in line with the ridge, are interpreted to be due to individual seamounts.

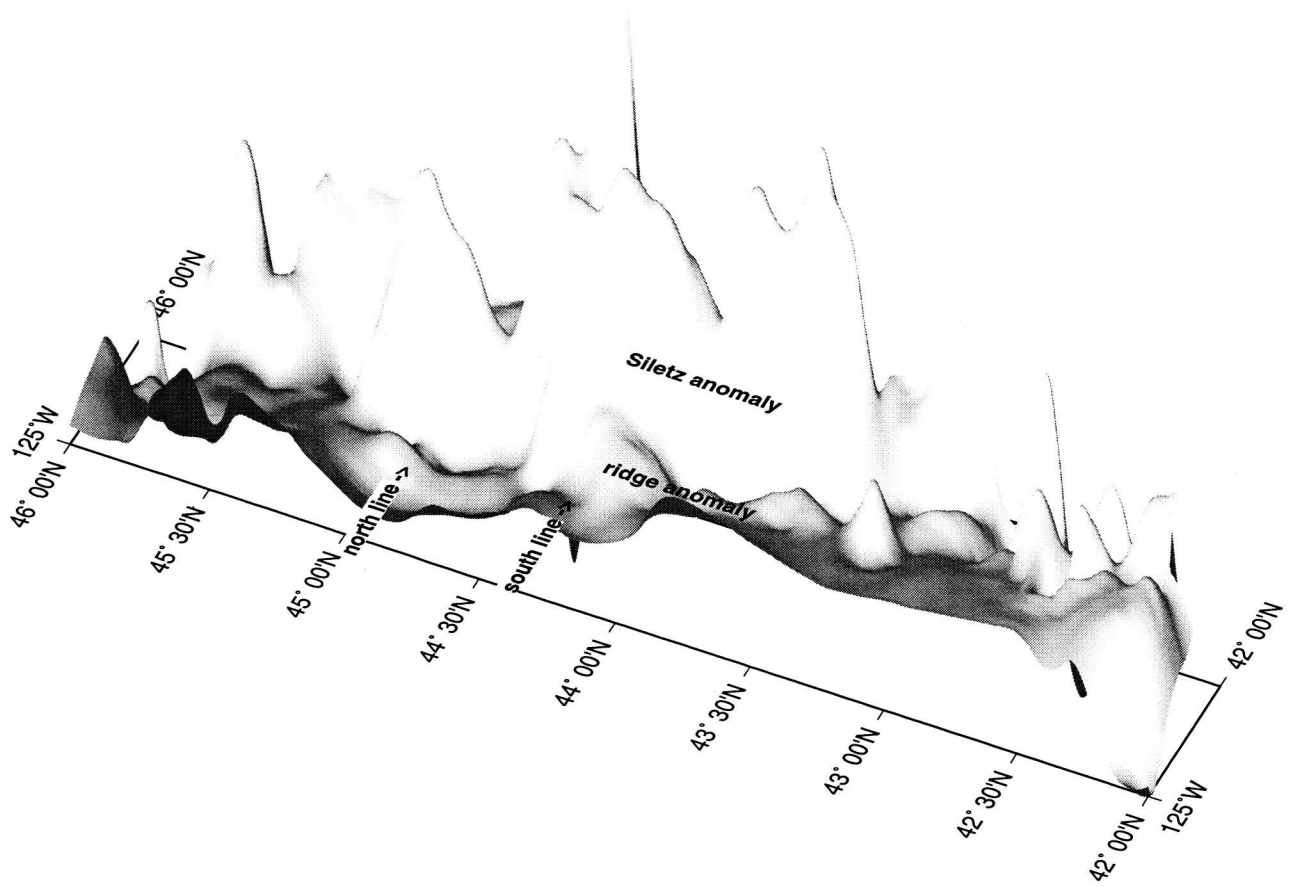
125°W
46° 00'N
46° 00'N
45° 30'N
45° 00'N
north line
44° 30'N
south line
44° 00'N
43° 30'N
43° 00'N
42° 30'N
42° 00'N
125°W
42° 00'N
Siletz anomaly
ridge anomaly

Figure 11

hill because such features are an order of magnitude too small (Macdonald et al., 1996) and also would not crosscut the pseudofault. In addition, neither of these features explains the observed velocity anomaly. The data can be explained by incorporating a block of Siletz terrane material, separated from and westward of the Siletzia backstop. However, the lack of a significant net $\mathbf{F_R}$ in the Siletz terrane results in a lower net **M**, so a large volume (or cross-sectional area, in our 2D model) of Siletz-type material is required to match the magnetic data. This gives a depth to the top of the feature too shallow to be consistent with the velocity model, and if densities similar to those within the continental basement are used, this large mass lies on the upper limit of what is consistent with the gravity data. Moreover, it is unlikely that a severed but coherent block of the Siletz terrane would be transported several kilometres seaward in a convergent margin.

The magnetic and gravity anomalies can be interpreted as the superposition of the responses of a number of slivers of oceanic crust obducted into the accretionary complex, as is observed offshore in the Franciscan complex of California. Seismic refraction techniques would identify these features as a single high velocity zone. Crossing of the anomaly over a pseudofault has no bearing on this interpretation. However, the magnetic anomaly is narrow, linear, and continuous over a distance of several hundred kilometres along the continental margin, which is not suggestive of a mass of crustal slivers obducted into the accretionary prism. The data can also be matched by a single, large piece of oceanic crust that has been thrust into the accretionary prism. Such features have been inferred to exist in the relict subduction

zone of the central California continental margin (Trehu, 1991) and in the active subduction zone of the S.E. Sulu Sea basin (Hinz et al., 1991). Such a thrust might originate from a margin-parallel zone of weakness created by bending of the JdF plate as it subducts. This interpretation is consistent with the general character of the magnetic anomaly and is not invalidated by the presence of the pseudofault. However, evidence for the existence of such features remains scant. Finally, the data may be matched by an aseismic ridge. Crossing of the anomaly over the pseudofault implies that the ridge formed far away from a spreading ridge, which is difficult to explain. However, such a feature is consistent with both the general character of the 2D anomaly and the inferred presence of seamounts at the southern margin of the anomaly, so we have chosen to tentatively interpret the model in this manner. Clearly, though, all the possible interpretations have problems, and the existing data are inadequate to resolve the issue.

If the magnetic anomaly is attributed to obducted oceanic crust or an aseismic ridge, the remnant field of the feature must be normally polarized, because a reversed $|\mathbf{M_R}|$ would result in a negative anomaly (if $\mathbf{F_R} > \mathbf{F_I}$) or would require too much mass to satisfy the gravity data and external geologic constraints (if $\mathbf{F_R} < \mathbf{F_I}$). We must also explain why these materials have retained their magnetic properties while the JdF crust has become largely demagnetized. The very low values for K and $|\mathbf{M_R}|$ determined for the JdF basalts in the magnetic quiet zone are bulk values for the JdF plate as a whole. If demagnetization occurred as a result of heating from below, then the upper surface

of the subducting plate, where the aseismic ridge and seamounts lie or from which the obducted oceanic crust originated, would retain its magnetization.

The incorporation of a body to explain the linear anomaly slightly modifies the magnetic background against which the Siletz terrane is modelled. As a result, in the model of figure 6 the Siletz edge dips 40° to 49° seaward to a depth of ~9 km, as opposed to the value of 55° calculated in our dip versus susceptibility analysis.

4.2 South Line, 44°11'N

4.2.1 Model Geometry and Parameterization

Our model of the north line, where significant external geological and geophysical constraints are available, served as a key to interpreting the magnetic and gravity data along the southern transect, where fewer seismic constraints are available. Our current working model of the Oregon convergent margin at 44°11'N is given in figure 12. Density, K, $|M_R|$, D, and I for each body in the model are given in table 2.

The regional magnetic map shows that the magnetic lineaments of the JdF plate are uninterrupted between the two profiles in this study. This suggests that the JdF plate in the area of consideration is not broken into segments with significantly different dips beneath the accretionary complex. We therefore assume the same JdF plate geometry for our starting model of the southern transect.

Figure 12. Potential field model of Oregon convergent margin, 44°11'N (south line). Model parameters are given in Table 2. Body 1: water; bodies 2, 4, 6, 11: accretionary complex; 3: accretionary complex and oceanic sediments; 5: upper Eocene volcanics; 7-9: continental basement; 10: aseismic ridge or seamount; 12-35: JdF crust; 36: oceanic mantle. VE=2.

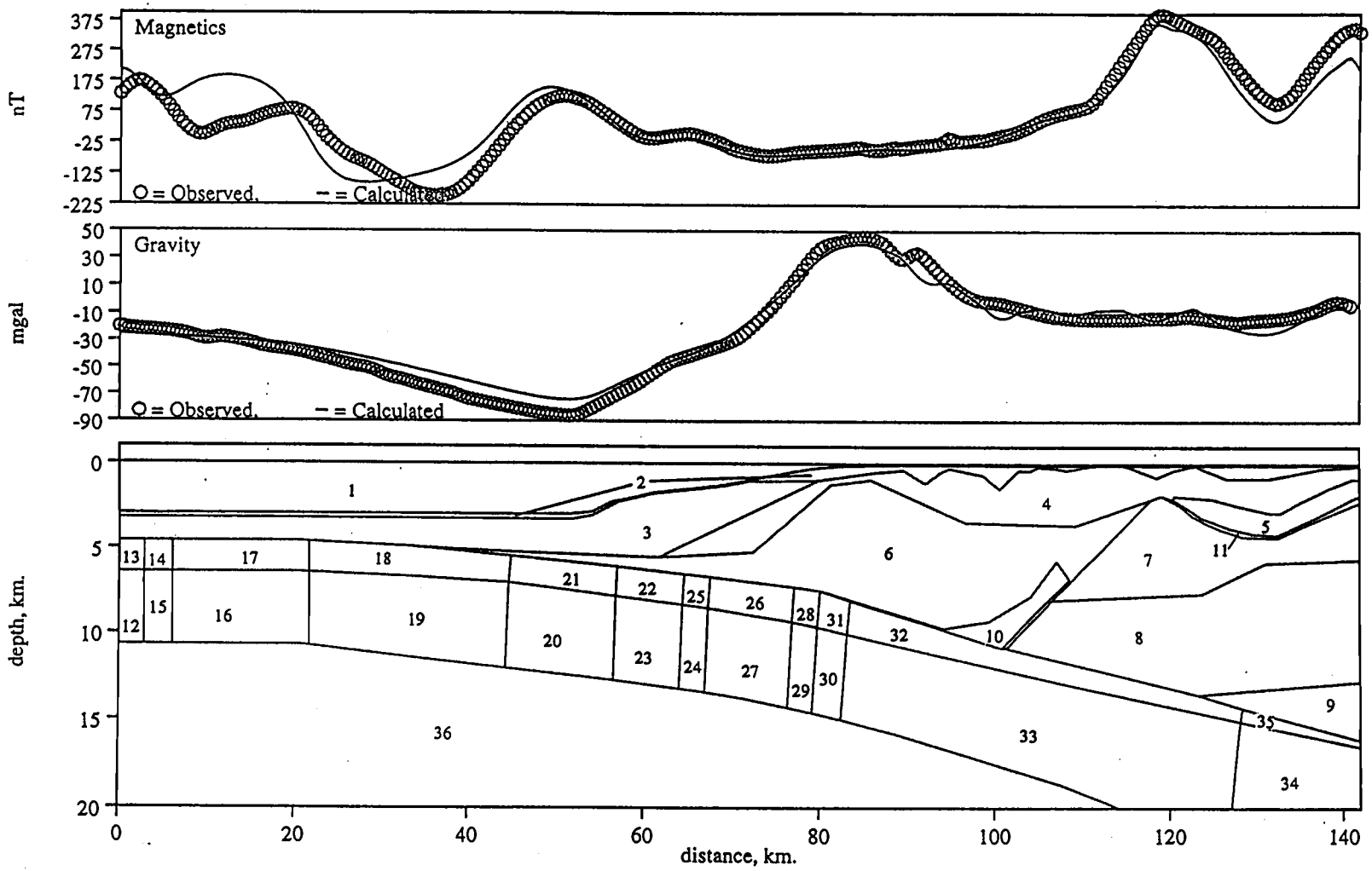
Magnetics
nT
375
275
175
75
-25
-125
-225
O = Observed,
– = Calculated
Gravity
mgal
50
30
10
-10
-30
-50
-70
-90
O = Observed,
– = Calculated
depth, km.
0
5
10
15
20
1
2
3
4
5
6
7
8
9
10
11
12
13
14
15
16
17
18
19
20
21
22
23
24
25
26
27
28
29
30
31
32
33
34
35
36
0
20
40
60
80
100
120
140
distance, km.

Figure 12

Body	Density (g/cc)	K (cgs units)	|Mr| (emu/cm3)	D (degrees)	I (degrees)	Geology
1	1.024	0	0	-	-	water
2	1.8	0	0	-	-	shallow basin fill
3	2	0	0	-	-	oceanic and prism sediments
4	2.28	0	0	-	-	accretionary prism sediments
5	2.75	0.0026	0.00125	46	64	upper Eocene basalt
6	2.54	0	0	-	-	compacted prism sediments
7	2.6	0.0033	0	-	-	upper Siletz terrane
8	2.72	0.0033	0	-	-	middle Siletz terrane
9	3.1	0.0033	0	-	-	lower Siletz terrane
10	2.7	0.003	0.001	19	69	aseismic ridge
11	2.35	0	0	-	-	sediments
12	2.95	0.003	0.001	19	69	lower Juan de Fuca plate
13	2.65	0.003	0.001	19	69	upper Juan de Fuca plate
14	2.65	0.002	-0.001	19	69	upper Juan de Fuca plate
15	2.95	0.002	-0.001	19	69	lower Juan de Fuca plate
16	2.95	0.0018	0.0008	19	69	lower Juan de Fuca plate
17	2.65	0.0018	0.0008	19	69	upper Juan de Fuca plate
18	2.65	0.002	-0.0013	19	69	upper Juan de Fuca plate
19	2.95	0.002	-0.0013	19	69	lower Juan de Fuca plate
20	2.95	0.0017	0.0007	19	69	lower Juan de Fuca plate
21	2.65	0.0017	0.0007	19	69	upper Juan de Fuca plate
22	2.65	0.0019	-0.0008	19	69	upper Juan de Fuca plate
23	2.95	0.0019	-0.0008	19	69	lower Juan de Fuca plate
24	2.95	0.0019	0.001	19	69	lower Juan de Fuca plate
25	2.65	0.0019	0.001	19	69	upper Juan de Fuca plate
26	2.65	0.0018	-0.0007	19	69	upper Juan de Fuca plate
27	2.95	0.0018	-0.0007	19	69	lower Juan de Fuca plate
28	2.65	0.001	0.0005	19	69	upper Juan de Fuca plate
29	2.95	0.001	0.0005	19	69	lower Juan de Fuca plate
30	2.95	0.001	-0.0005	19	69	lower Juan de Fuca plate
31	2.65	0.001	-0.0005	19	69	upper Juan de Fuca plate
32	2.65	0.001	0.0005	19	69	upper Juan de Fuca plate
33	2.95	0.001	0.0005	19	69	lower Juan de Fuca plate
34	2.95	0	0	-	-	lower Juan de Fuca plate
35	2.65	0	0	-	-	upper Juan de Fuca plate
36	3.2	0	0	-	-	oceanic mantle

Table 2. Model parameters for south line (figure 12)

The best available constraint on the structure of the accretionary prism and backstop at this latitude on the continental margin is the cross-section of Snavely et al. (1985), who considered MCS reflection lines, regional gravity and magnetics data, an industry well, and onshore surficial geology. The cross-section is not exactly coincident with the potential field profile we are modelling, but examination of variously-oriented seismic lines in this area did not reveal significant changes in regional geology over the small distances between the two data sets. The shallow basin structure of the cross-section was projected onto the plane of our model, as was the distribution of the upper Eocene Yachats basalt (visible on the regional magnetics map as a strong, localized high where it outcrops at the coast at ~44°15'N; adjacent strong, areally limited lows immediately to the north probably represent the same basalt outcrop, but reversely magnetized). Snavely's interpretation of the geometry of the top of the Siletz terrane was also adopted as a starting point for our modelling efforts. We used the bathymetry data collected simultaneously with the shiptrack magnetic and gravity data. Both the general density structure within the accretionary prism and the geometry of the edge of the Siletz terrane from our modelling of the northern line were also used as a starting point for this model.

D and I of the upper Eocene basalts were set to 46° and 64°, respectively (Simpson and Cox, 1977), and initial estimates of K and $|\mathbf{M_R}|$ for all model bodies were taken from Bromery and Snavely (1964) and the modelling results of the north line. The assumptions and conclusions we previously made with respect to the magnetic properties of Siletzia and their relationship to cross-sectional geometry are

valid at crustal scales and thus were again used at this location. Siletz bulk $|\mathbf{M_R}|$ was again set to zero and we used an initial bulk K of 0.00285 cgs units, the value from our model of the north line.

4.2.2 Modelling Results

Matching the response of the JdF plate to the observed magnetic quiet zone again required inclusion of a progressive eastward demagnetization of the oceanic crust.

Magnetic modelling required a lesser depth to the top of the Siletz terrane where it lies under the Yachats Basalt than suggested by Snavely et al. (1985). The short-wavelength features superimposed on the Siletz anomaly at model km 130 to 160 clearly reflect the relatively well-known spatial distribution of the upper Eocene basalt and are easily modelled. The best-fit dip of the western edge of Siletzia is somewhat shallower than to the north (28°), and the best-fit bulk K was similar at 0.0033 cgs units, again assuming a straight-line configuration in cross-section.

A small-amplitude, medium-wavelength magnetic anomaly is clearly superimposed on the main Siletz anomaly at model km 100 to 110 (figure 12, III on figure 3a). Locally, this anomaly may be adequately modelled as topographic relief on the lower portion of the generally west-dipping Siletz edge. However, examination of magnetic anomaly maps (figures 3a and 11) reveals this feature to be part of the long, linear magnetic anomaly that parallels much of the Oregon convergent margin and which we have tentatively attributed to an aseismic ridge (see previous discussion). This narrow,

linear anomaly partially merges with the larger Siletz response in the vicinity of Heceta Bank. If the linear anomaly is modelled as an aseismic ridge and if the Siletz backstop does indeed have a straight-line configuration in cross-section, then the magnetic data require that the ridge is colliding with the backstop. Our model includes a ridge that is being scraped off the subducting JdF plate by the strong, massive basaltic backstop, which is also consistent with the gravity data. An acceptable alternative model includes a ridge beginning to be subducted beneath the backstop, pushing the Siletz rocks upward.

In a general sense, the densities of various geologic units and their distribution determined by gravity modelling of the northern line work well at this location. Densities again tend to increase downward and arcward within both the accretionary prism and the Siletz terrane. However, the gravity data require a mass excess in the vicinity of Heceta Bank. The magnitude of the Heceta Bank high (~50 mgal; figures 3b and 12) can not be explained by the interplay of topography, shallow basins, the subducting JdF plate, constraints from magnetics modelling, and an accretionary prism having either the same internal density structure as the northern transect or a single homogenous density (refer to figure 13 and its caption). A mass concentration must be incorporated into the model, but there is clearly a trade-off between density and volume. At one extreme, a high-density (~2.7 g/cc) but volumetrically small mass concentration at great depth, floored by the JdF plate, adequately models the gravity high. A feature of this density would most likely consist of oceanic basalt (a seamount is a likely candidate), which would result in a magnetic anomaly. No such

Figure 13. Comparison of observed gravity field to that predicted by three preliminary models. *Continuous line:* observed gravity field, south line. Heceta Bank anomaly is large high from km ~75 to ~100. *Filled grey squares:* response of simple model including JdF plate (uniform density of 2.85 g/cc, geometry of figures 2 and 6), oceanic mantle (uniform density of 3.2 g/cc from velocity model of figure 2), NA moho (depth of 40 km from Li, 1996), NA mantle (uniform density of 3.1 g/cc from Li, 1996 and gravity model of north line), and uniform NA crustal density of 2.65 g/cc (Bouguer replacement density). Model illustrates edge effect due to interference between the responses to shallowing topography and deepening oceanic crust, using known geometries and densities for major crustal elements. Edge effect gives large high in vicinity of Heceta Bank, but calculated peak is ~10 km westward of observed peak, and mismatch in eastern side of model is very large. As bathymetry and JdF geometry are well-known, lateral mispositioning of peak suggests that the edge effect (which is a function of these two parameters) is not the main source of the Heceta Bank anomaly. Absence of high-density mafic continental basement invalidates the model even as a first approximation. *Open circles:* Additional constraints are applied to the model, including topography, shallow basins (Snavely et al., 1985), subducting JdF plate, and constraints from magnetics modelling. Accretionary prism below the shallow basins is given a homogenous density of 2.35 g/cc. Agreement of modelled response to data is increased dramatically toward the east and on the western flank of the Heceta Bank anomaly. A significant mismatch exists at the location of the Heceta Bank anomaly itself. *Filled stars:* All available external information is applied to the model. This is identical to model denoted by the open circles, except that internal density structure of the accretionary prism determined from velocity and gravity modelling of the north line is incorporated here. Fit improves dramatically, but the calculated response still underestimates the gravity field at Heceta Bank by ~25 mgal. A mass excess is required within Heceta Bank. *Dashed line:* response of the model given in figure 12.

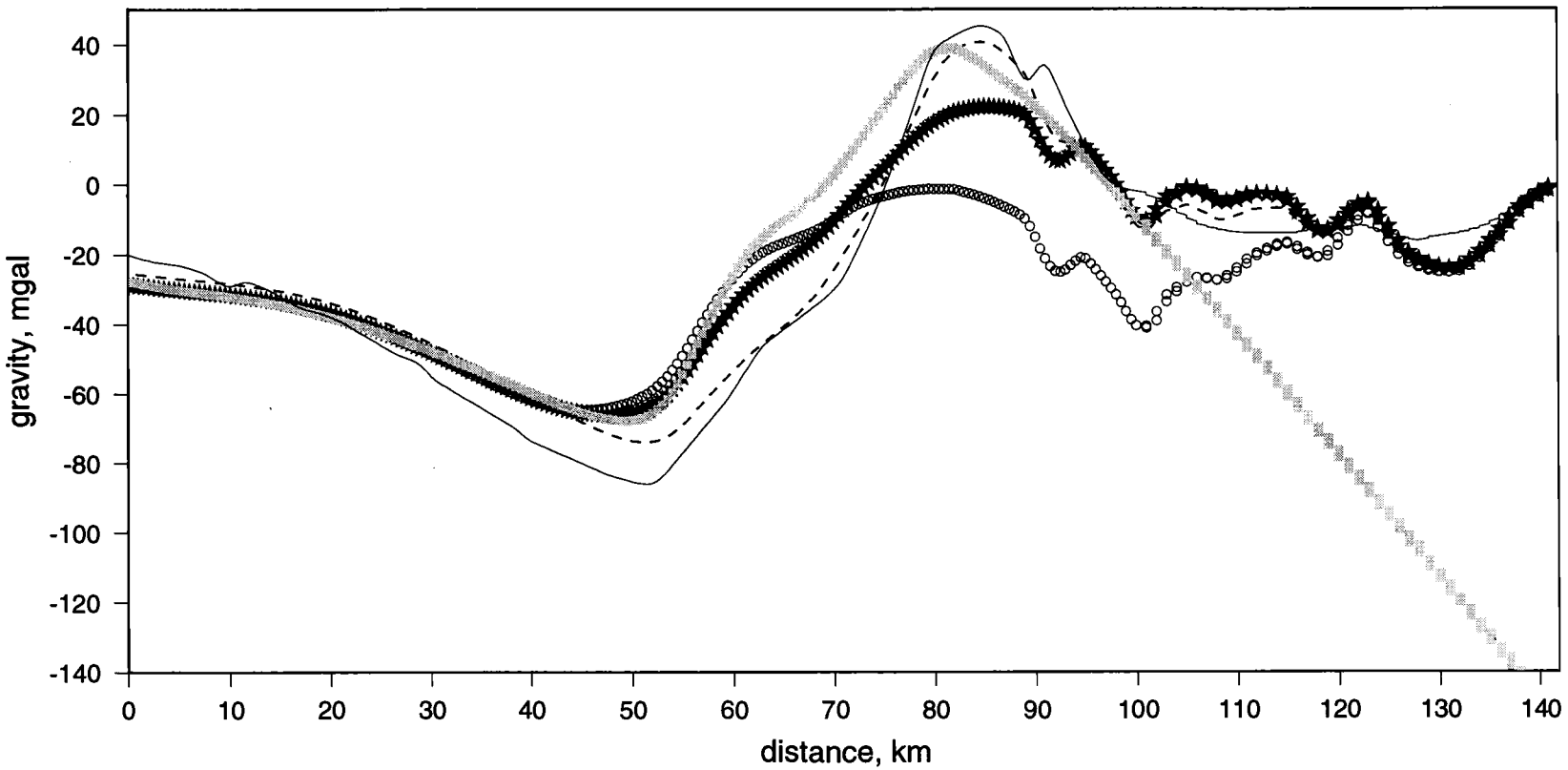
gravity, mgal
40
20
0
-20
-40
-60
-80
-100
-120
-140
0
10
20
30
40
50
60
70
80
90
100
110
120
130
140
distance, km

Figure 13

anomaly is observed over Heceta Bank. If the seamount has a reversed remnant magnetization and K and $|\mathbf{M_R}|$ are such that $\mathbf{F_R}$ balances $\mathbf{F_I}$ exactly, a "stealth" seamount with little or no magnetic signature would result. This is not quite as contrived as it may at first appear, as the remnant and induced field directions for this part of the JdF crust are parallel and the Koenigsberger ratio may be ~1 for these basalts. For reversely magnetized rock, this would theoretically result in such a balance between the two fields. However, the likely variability in magnetic properties that would exist within such a feature should result in a small magnetic signal.

While the stealth seamount hypothesis can not be firmly ruled out, it is more probable that the relatively high-density sediments (2.54 g/cc) seaward of the continental backstop, which rose to a depth no shallower than ~2.5 km in our model of the north line (body 6 in figure 6), rise here to form a high-density core to Heceta Bank (body 6 in figure 12). This is consistent with the preliminary findings of Flueh et al. (1996), whose seismic refraction work suggests relatively high velocities shallow within Heceta Bank.

5. DISCUSSION

5.1 Backstop Geometry, Accretionary Prism Deformation, Stress Fields, and Theoretical Models of Forearc Deformation: A Synthesis

All available evidence suggests that the seaward edge of the Siletz terrane serves as a major E-W boundary separating regions with different stress regimes and deformational styles. In this section, we argue that this is generally consistent with theoretical models of forearc deformation.

Our potential field models reliably show that the Siletz backstop dips seaward to a depth of at least ~7 km. While the nature of forearc deformation is also dependent on the rheology of prism sediments, it is reasonable to suggest that a such a large seaward-dipping ramp of strong basaltic rock might serve to push the accretionary prism sediments up and over it, like a bulldozer blade or snow shovel. Generic models of backstop-accretionary prism interaction tend to confirm this (e.g. Wang and Davis, 1996). MCS reflection data coincident with the potential field transects of this study, however, do not show significant thrust faulting over the western edge of the Siletz terrane, although there is evidence for a blind reverse fault over the Siletz backstop beneath Stonewall Bank (Robert Yeats, pers. com., 1996). Instead, accretionary prism deformation associated with the edge of the Siletz terrane appears to be primarily strike-slip, with secondary thrusting (see discussion below of the Fulmar and Nehalem Bank faults). In addition, interpretations of seismic and well data in the Oregon continental margin indicate that thrust faulting is ubiquitous

throughout the accretionary prism west of the edge of the Siletz terrane, but absent to the east (Snavely et al., 1980, 1985). Moreover, the strike-slip faults in the Oregon accretionary prism identified by Goldfinger et al. (in press) terminate at the seaward edge of the Siletz terrane (figure 4).

Both the N-S strike of anticlines and thrust faults (Werner et al., 1991) and the NW-SE trending left lateral strike-slip faults in the accretionary complex offshore Oregon indicate that the maximum horizontal compressive stress is oriented E-W (figure 4). In contrast, the orientation of maximum horizontal compressive stress in the forearc east of the seaward edge of the Siletz terrane is N-S (e.g. Werner et al., 1991; Zoback, 1992; figure 4). Wang (1996) suggested that the Oregon and Washington forearc is moving northward along an inferred dextral shear zone in the Cascade volcanic arc in response to oblique subduction of the JdF plate, and is colliding in the north with a buttress apparently consisting of the massive batholith of the Canadian Coast Range, producing the observed N-S stress orientation.

The Fulmar fault lies approximately over the western edge of the Siletz terrane and is interpreted to strike margin-parallel with dextral slip (Snavely et al., 1980, 1985; Snavely, 1987; Trehu et al., 1994, 1995; see figure 4). It is conceivable that the narrow band of short-wavelength, margin-parallel folds observed over the western edge of the Siletz terrane in central Oregon (Charles Hutto, pers. com., 1996) may be the expression of a compressive component of stress on this fault. The trend and sense of strike-slip motion inferred for the Fulmar fault result from a maximum horizontal

compressive stress oriented approximately NE-SW (e.g. Turcotte and Schubert, 1982, p. 350, 357), consistent with the plate convergence direction. The predominantly N-S trending dextral Nehalem Bank fault, which lies northward of the northernmost mapped extent of the Fulmar fault and extends to Willapa Bay in southernmost Washington, might be an en echelon structure to the Fulmar fault (figure 4). Note that the eastward step-over of dextral, margin-parallel faulting from the Fulmar fault in the south to the Nehalem Bank fault in the north occurs at about the same location along the coast (~45°30'N) that the thick, rigid Siletz backstop turns inland (figure 4).

The observations listed above are consistent with the theoretical models of forearc deformation calculated by Platt (1993). Platt demonstrated that for a high obliquity of subduction, regardless of accretionary prism rheology, deformation reflects a trench-normal stress field through most of the accretionary wedge (in our case, N-S striking anticlines and thrust faults and NW-SE striking left-lateral strike-slip faults), with trench-parallel motion confined to a shear zone or strike-slip fault (the Fulmar and Nehalem Bank faults) within the wedge where it contacts the backstop (the western edge of the Siletz terrane). The N-S component of stress appears to be primarily transmitted with little associated deformation to the Siletz terrane, leading to the collision of the forearc sliver with a buttress to the north and producing the observed N-S maximum horizontal compressive stress direction (Wang, 1996). The N-S stress component may also be partly relieved by motion of the wedge as a whole northward along the Fulmar and Nehalem Bank faults, although the absence of extensional features at the stepover between the faults (figure 4) suggests that the magnitude of

this motion is probably not large. Undoubtedly, other factors, such as variation in sediment supply, also contribute to changes in deformational style (e.g. MacKay, 1995), but neotectonic and stress data indicate that Platt's model provides a self-consistent general framework for deformation in the Oregon accretionary prism.

The three-dimensionality of the thick Siletz terrane block of central Oregon (figures 3a, 3b, and 4) also leads to a transition across its northern margin in the style of deformation within the accretionary prism. McNeill et al. (submitted) partially attributed gravity-induced normal faulting in the Washington accretionary complex and the increased width and lower taper angle of the Washington and northern Oregon margins relative to those of central Oregon to the absence of rigid Siletz basement. However, N-S changes in deformational style within the accretionary complex due to corresponding changes in the thickness of Siletzia are less obvious than the E-W transition in deformational style across the Siletz terrane's western edge, probably because any backstop, including the much weaker one of the Washington accretionary prism, will produce some of the same effects. The strike-slip faults in the Oregon accretionary prism mapped by Goldfinger et al. (1992, in press) appear to diminsh drastically in number in northern Oregon and Washington, and no significant N-S trending strike-slip faults analagous to the Fulmar and Nehalem Bank faults have been identified north of Willapa Bay. The relative absence of such mapped faults to the north of the thick Siletz block suggests that margin-parallel changes in the backstop affect deformational style in the accretionary prism, but it may also reflect the lesser degree of study of the Washington continental margin (L.D. Kulm, pers. com., 1996).

Nonetheless, it is clear that the Siletz terrane is a major control of crustal deformation in the Pacific Northwest and that the nature and geometry of a backstop is in general a major controlling factor in accretionary prism dynamics. These two observations have not yet been combined in a rigorous manner to determine the precise implications of the geometry of the Siletz edge that we have inferred for the central Oregon margin. The main achievement of our modelling efforts is to constrain backstop geometry and thus provide additional information to be used in geodynamic models. A recalculation of the thermal models of Hyndman and Wang (1993) and Oleskevich (1994) using our Siletz geometry would be valuable. An application of the mathematical model of Shrieve and Cloos (1986) using our Siletz geometry constraints as input would also be illuminating. This model, however, is two-dimensional, whereas basement structure and backstop geometry, sediment supply, and plate motions are highly three-dimensional in Cascadia. The most useful type of future work would consist of three-dimensional modelling using finite element analysis or scaled sandbox models, incorporating a simplified representation of the three-dimensional shape of the Siletz backstop.

5.2 Heceta Bank

We conclude that Heceta Bank is cored by material with a density consistent with the compacted sedimentary rock inferred to generally occur deep in the accretionary prism (body 6 in figures 6 and 12), suggesting that this material has been tectonically uplifted locally. While the NW-trending, left-lateral Heceta Bank Fault appears to delimit the southern limit of the bank, there is no evidence of a transpressive regime

here (L.D. Kulm, pers. com., 1996). Kulm and Fowler (1974) found evidence for as much as 1000 m of tectonic uplift in the western part of Heceta Bank, and suggested that the observed underthrusting of Pleistocene abyssal plain and fan deposits beneath the earlier Cenozoic rocks underlying the continental shelf might be responsible for this uplift. It is probable that the older, compacted sedimentary rocks beneath the shelf were thus pushed upward by the underthrusted sediments to form the high-density core of our gravity model.

At km ~95 to ~110 of our gravity model (figure 12), the relatively high-density pocket (body 6) lies ~600 m deeper than it does in the northern transect (body 6 in figure 6), and it lies ~1 km deeper than the edge of the backstop, behaviour also not seen in our model of the north line. This is consistent with Kulm and Fowler's (1974) observation of subsidence in the inner continental shelf, and suggests that the relative uplift of the high-density sediments to the west, forming the Heceta Bank core, was also in part a result of downdropping of these high-density sediments to the east.

Nehalem Bank, which appears to be structurally and dimensionally comparable to Heceta Bank (Kulm and Fowler, 1974), has no associated large gravity high (figure 3b), indicating that it does not contain the high-density core interpreted to exist within Heceta Bank. One explanation is that the deep sediments underlying Nehalem Bank are simply less dense than their counterparts in the vicinity of Heceta Bank, perhaps due to less compaction and/or lithological differences (L.D. Kulm, pers. com., 1996). The lack of a strong Siletz backstop at the latitude of Nehalem Bank (figure 3a) might

contribute to a lesser degree of compaction, and the nearby presence of the Columbia River might contribute to differences in grain size and chemistry. Alternatively, Heceta Bank's high-density core may result from collision of a subducted ridge with the continental backstop (figure 12). Inspection of magnetic anomaly maps (figures 3a and 11) reveals that the only point along the Oregon continental margin where the ridge closely approaches or contacts the backstop is in the vicinity of Heceta Bank. The ridge clearly remains west of continental basement elsewhere, including our northern line. Shelf sediments are uplifted above the colliding Daiichi Kashima seamount in the Japan Trench (Lallemand and Le Pichon, 1987). While our proposed ridge is smaller, a similar effect could be occurring at Heceta Bank, causing deeper, denser sedimentary rock to be tectonically uplifted to form a core and leading to uplift of the shelf as a whole. In earlier stages of seamount subduction, uplift occurs but topographic relief on the continental shelf is less extreme (Lallemand and Le Pichon, 1987) and a high-density core might not be formed; this may correspond to our northern transect and to the more subdued bathymetry south of Heceta Bank. Along-strike variations in the size of the ridge could also play a significant role in the degree of associated accretionary prism deformation.

Alternatively, if the ridge is being scraped off the JdF plate by the high-strength Siletz backstop, then perhaps the ridge material is acting as a barrier, inhibiting sediment subduction by blocking the subduction channel. This could cause subducting sediment to pile up to the west, forcing deep, dense sedimentary rocks in the accretionary prism upwards. Such an effect would not be seen north or south of

Heceta Bank, where the ridge is not in contact with the backstop. Note that blockage of the subduction channel might also be accomplished by a large piece of oceanic crust thrust into the accretionary prism, which is an alternate interpretation of the linear magnetic anomaly which we have tentatively attributed to an aseismic ridge.

The banks along the Oregon continental margin may be viewed as classic outer arc highs (L.D. Kulm, pers. com., 1996). However, it remains poorly understood why this outer arc high exists as a number of discrete banks rather than as a continuous bathymetric and structural feature along the entire margin. The existence of Nehalem Bank as a distinct feature might be explained by the high sedimentation rate near the mouth of the Columbia River, but no major margin-parallel increase in sedimentation rate is associated with the other banks, including Heceta Bank. One explanation is that the deformation leading to bank formation is more ubiquitous than might be inferred from consideration of large-scale bathymetric features alone. A number of smaller banks interpreted to be structurally similar to Heceta and Nehalem Banks (Kulm and Fowler, 1974) are scattered along the Oregon continental margin, and seaward-verging thrusts in the continental slope are producing rapidly uplifting ridges which may eventually form new submarine banks (L.D. Kulm, pers. com., 1996, Shipboard Scientific Party, 1994). This implies that Heceta and Nehalem Banks are simply larger examples of processes which occur throughout the Oregon continental margin.

We offer here an observation which we speculate might have some bearing on the formation of these banks. We inferred the presence of a discontinuity in JdF spreading anomalies in the vicinity of Heceta Bank (see previous chapter). The age of the JdF crust to the north of this presumed pseudofault, at the coastline, is about 11 Ma. We estimate the age of JdF crust to the south of this discontinuity to be about 7 Ma. Calculation of seafloor depths north and south of the pseduofault from these ages on the basis of the gradual cooling and subsidence of oceanic lithosphere (e.g. Turcotte and Scubert, 1982, p. 182) gives a difference in ocean floor depth across the pseudofault of 244 m. The next large submarine bank to the north is Nehalem Bank. A linear projection across the magnetic quiet zone of the next JdF pseudofault to the north places its intersection with the coast at Nehalem Bank. With a difference in age of only ~1 Ma, the difference in depth to the JdF crust across this pseudofault is smaller than that estimated in the vicinity of Heceta Bank.

The points of intersection between these pseudofaults and the coast have probably remained approximately stationary for the life of both banks, because the trend of both pseudofaults is roughly parallel to the direction of relative plate motion between the JdF and NA plates (Riddihough, 1984), which has not changed much over the last several million years (Wilson, 1988). The topographic breaks due to pseudofaults in the JdF crust must nonetheless plow through the sediments of the accretionary prism due to both northward movement of the accretionary complex west of the backstop and trench-normal compression within the prism (see Section 5.1). However, the

process whereby differences in depth to the oceanic crust might lead to structural features such as Heceta and Nehalem Banks remains unclear.

6. CONCLUSIONS

Magnetic and gravity modelling in conjunction with external geologic and geophysical constraints indicates that the backstop-forming western side of the Siletz terrane has a seaward dip of about 40° to 49° at 44°48'N on the Oregon continental margin, shallowing to ~28° at 44°11'N. This is a well-determined result, given available a priori information, to a depth of ~7 km. The Siletz terrane may continue to descend at these dips to the subducting JdF plate, but alternate geometries for the lowermost portion of the backstop are also consistent with the potential field data. The magnetic data also require progressive eastward demagnetization of the JdF crust in the magnetic quiet zone, which is most likely due to heating of the subducting oceanic plate to the Curie temperature but may also result from hydrothermal alteration.

Our southern transect reveals that Heceta Bank is cored by relatively high-density sediments (~2.54 g/cc), consistent with the model proposed by Kulm and Fowler (1974) for submarine bank formation in the Oregon convergent margin. On the basis of magnetic, gravity, and velocity data, we interpret an aseismic ridge to be present beneath the accretionary complex from about 45°N to 42°N. This ridge may collide with the backstop beneath Heceta Bank and may play a role, in concert with imbricate thrust faulting, in the formation of Heceta Bank's high-density core. We also speculate that an estimated difference in depth to the JdF plate of several hundred metres due the juxtaposition of different-aged oceanic crust across pseudofaults which intersect the

coast at the latitudes of Heceta and Nehalem Banks may be another factor in the construction of these topographic highs.

The backstop geometry we derive, when combined with other structural, neotectonic, and stress data, is consistent with a model of central Oregon forearc tectonics in which the backstop serves a major E-W boundary between stress regimes and deformational styles, in agreement with the generic models of accretionary wedge dynamics of Platt (1993). This 3D backstop geometry could be used as input to geodynamic models to gain further insight into the dynamics of accretionary prism deformation in this complex and poorly understood convergent margin.

BIBLIOGRAPHY

Blakely, Richard J., Extent of Partial Melting Beneath the Cascade Range, Oregon: Constraints from Gravity Anomalies and Ideal-Body Theory, *Journal of Geophysical Research,* v. 99, pp. 2757-2773, 1994.

Bromery, R.W., Snavely, P.D. Jr., Geologic Interpretation of Reconnaissance Gravity and Aeromagnetic Surveys in Northwestern Oregon, *U.S. Geological Survey Bulletin 1181-N,* 1964.

Butler, R.F., *Paleomagnetism: Magnetic Domains to Geologic Terranes*, 319 pp., Blackwell Scientific Publications, Boston, 1992.

Byrne, D.E., Wang, W., Davis, D.M., Mechanical Role of Backstops in the Growth of Forearcs, *Tectonics*, v. 12, pp. 123-144, 1993.

Cady, W.M., Tectonic Setting of the Tertiary Volcanic Rocks of the Olympic Peninsula, Washington, *U.S. Geological Survey Jour. Research*, v. 3, pp. 573-582, 1975.

Cande, Steven C., Kent, Dennis V., A New Geomagnetic Polarity Time Scale for the Late Cretaceous and Cenozoic, *Journal of Geophysical Research,* v. 97, pp. 13,917-13,951, 1992.

Cloos, Mark, Thrust-Type Subduction-Zone Earthquakes and Seamount Asperities: A Physical Model for Seismic Rupture, *Geology*, v. 20, pp. 601-604, 1992.

Cloos, Mark, Lithospheric Buoyancy and Collisional Orogenesis: Subduction of Oceanic Plateaus, Continental Margins, Island Arcs, Spreading Ridges, and Seamounts, *Geological Society of America Bulletin*, v. 105, pp. 715-737, 1993.

Coffin, Millard F., Eldholm, Olav, Scratching the Surface: Estimating Dimensions of Large Igneous Provinces, *Geology*, v. 21, pp. 515-518, 1993.

Cranswick, Doborah J., Piper, Kenneth A., Geologic Framework of the Washington-Oregon Continental Shelf - Preliminary Findings, *U.S. Geological Survey Circular 1092,* pp.146-151, 1991.

Davis, D.M., Suppe, J., Dahlen, F.A., Mechanics of Fold-and-Thrust Belts and Accretionary Wedges, *Journal of Geophysical Research,* v. 88, pp. 1153-1172, 1983.

Dmowska, Renata, Zheng, Gutuan, Rice, James R., Seismicity and Deformation at Convergent Margins due to Heterogeneous Coupling, *Journal of Geophysical Research*, v. 101, pp. 3015-3029, 1996.

Duncan, Robert A., A Captured Island Chain in the Coast Range of Oregon and Washington, *Journal of Geophysical Research*, v. 87, pp. 10,827-10,837, 1982.

Finn, C., Geophysical Constraints on Washington Convergent Margin Structure, *Journal of Geophysical Research*, v. 95, pp. 19,533-19,546, 1990.

Flueh, E., Fisher, M., and other cruise participants, 1996, Cruise Report S0 108, *ORWELL-GEOMAR Report 49*, Kiel, 251 pp.

Fowler, C.M.R., *The Solid Earth*, 472 pp., Cambridge University Press, New York, 1990.

Godfrey, N.J., Beaudoin, B.C., Klemperer, S.L., Ophiolitic Basement to the Great Valley Forearc Basin, California, from Seismic and Gravity Data: Implications for Crustal Growth at the North American Continental Margin, *Geological Society of America Bulletin*, in press.

Goldfinger, Chris, Active Deformation of the Cascadia Forearc: Implications for Great Earthquake Potential in Oregon and Washington, *PhD Thesis, Oregon State University*, 1994.

Goldfinger, Chris, Kulm, LaVerne D., Yeats, Robert S., Appelgate, Bruce, MacKay, Mary E., Moore, Gregory F., Transverse Structural Trends Along the Oregon Convergent Margin: Implications for Cascadia Earthquake Potential and Crustal Rotations, *Geology*, v. 20, pp. 141-144, 1992.

Goldfinger, Chris, Kulm, LaVerne D., Yeats, Robert S., McNeill, Lisa, Hummon, Cheryl, Oblique Strike-Slip Faulting of the Central Cascadia Submarine Forearc, *Journal of Geophysical Research*, in press.

Haeussler, Peter J., Bradley, Dwight, Goldfarb, Richard, Snee, Lawrence, Taylor, Cliff, Link Between Ridge Subduction and Gold Mineralization in Southern Alaska, *Geology*, v. 23, pp. 995-998, 1995.

Hinz, Karl, Block, Martin, Kudrass, Hermann Rudolf, Meyer, Heinrich, Structural Elements of the Sulu Sea, Philipines, *Geol. Jb.*, v. A 127, pp. 483-506, 1991.

Hubbert, M.K., A Line-Integral Method of Computing the Gravimetric Effects of Two-Dimensional Masses, *Geophysics*, v. 13, pp. 215-225, 1948.

Hyndman, R.D, The Lithoprobe Corridor Across the Vancouver Island Continental Margin: The Structural and Tectonics Consequences of Subduction, *Canadian Journal of Earth Science*, v. 32, pp. 1777-1802, 1995.

Hyndman, R.D., Wang, K., Thermal Constraints on the Zone of Major Thrust Earthquake Failure: The Cascadia Subduction Zone, *Journal of Geophysical Research,* v. 98, pp. 2039-2060, 1993.

Kelleher, John, McCann, William, Buoyant Zones, Great Earthquakes, and Unstable Boundaries of Subduction, *Journal of Geophysical Research,* v. 81, pp. 4885-4896, 1976.

Kelsey, Harvey M., Ticknor, Robert L., Bockheim, James G., Mitchell, Clifton E., Quaternary Upper Plate Deformation in Coastal Oregon, *Geological Society of America Bulletin,* in press.

Kulm, L.D., Fowler, G.A., Oregon Continental Margin Structure and Stratigraphy: A Test of the Imbricate Thrust Model, in *The Geology of Continental Margins,* ed.: C.A. Burke and C.L. Drake, pp. 261-283, Springer-Verlag, N.Y., N.Y., 1974.

Lallemand, Serge, Le Pichon, Xavier, Coulomb Wedge Model Applied to the Subduction of Seamounts in the Japan Trench, *Geology*, v. 15, pp. 1065-1069, 1987.

Li, Xiao-Qing, Deconvolving Orbital Surface Waves for the Source Duration of Large Earthquakes and Modeling the Receiver Functions for the Earth Structure beneath a Broadband Seismometer Array in the Cascadia Subduction Zone, *PhD Thesis, Oregon State University,* 1996.

MacDonald, Ken C., Fox, P.J., Alexander, Russ T., Pockalny, Robert, Gente, Pascal, Volcanic Growth Faults and the Origin of Pacific Abyssal Hills, *Nature*, v. 380, pp. 125-129, 1996.

MacKay, Mary E., Structural Variation and Landward Vergence at the Toe of the Oregon Accretionary Prism, *Tectonics*, v. 14, pp. 1309-1320, 1995

Magill, J., Cox, A., Duncan, R., Tillamook Volcanic Series: Further Evidence for Tectonic Rotation of the Oregon Coast Range, *Journal of Geophysical Research*, v. 86, pp. 2953-2970, 1981.

McCaffrey, Robert, Goldfinger, Chris, Forearc Deformation and Great Subduction Earthquakes: Implications for Cascadia Offshore Earthquake Potential, *Science*, v. 267, pp. 856-859, 1995.

McNeill, Lisa C., Piper, Kenneth A., Goldfinger, Chris, Kulm, LaVerne D., Yeats, Robert S., Listric Normal Faulting on the Cascadia Continental Margin, *Journal of Geophysical Research,* submitted.

Milsom, John, *Field Geophysics,* 182 pp., Open University Press, Milton Keynes, 1989.

Oleskevich, D.A., Comparison of Thermal Constraint Modelling on Selected Profiles Along the Cascadia Subduction Zone, *University of Victoria Department of School of Earth and Ocean Sciences work term report,* 1994.

Parker, Robert L., *Geophysical Inverse Theory*, 386 pp., Princeton University Press, Princeton, New Jersey, 1994.

Peacock, Simon M., Thermal Effects of Metamorphic Fluids in Subduction Zones, *Geology*, v. 15, pp. 1057-1060, 1987.

Peterson, C.P., Loubere, P.W., Lulm, L.D., Peper, J.S., Stratigraphy of Continental Shelf and Coastal Region, in *Western North American Continental Margin and Adjacent Ocean Floor off Oregon and Washington, Atlas 1, Ocean Margin Drilling Program Regional Atlas Series*, ed.: Kulm, L.D., sheet 8, Marine Science International, Woods Hole, Mass., 1984.

Platt, J.P., Mechanics of Oblique Convergence, *Journal of Geophysical Research,* v. 98, pp. 16,239-16,256, 1993.

Riddihough, R.P., Recent Movements of the Juan de Fuca Plate System, *Journal of Geophysical Research,* v. 89, pp. 6980-6994, 1984.

Sample, James C., Reid, Mary R., Tobin, Harold J., Moore, J. Casey, Carbonate Cements Indicate Channeled Fluid Flow Along a Zone of Vertical Faults at the Deformation Front of the Cascadia Accretionary Wedge (Northwest U.S. Coast), *Geology*, v. 21, pp. 507-510, 1993.

Scheidegger, K.F., Thermal Evolution of the Juan de Fuca Plate, in *Western North American Continental Margin and Adjacent Ocean Floor off Oregon and Washington, Atlas 1, Ocean Margin Drilling Program Regional Atlas Series,* ed.: Kulm, L.D., sheet 8, Marine Science International, Woods Hole, Mass., 1984.

Shedlock, K.M., Weaver, C.S., Program for Earthquake Hazards Assessment in the Pacific Northwest, *U.S. Geological Survey Circular 1067*, 1991.

Shipboard Scientific Party, 7. Site 892, in *Proceedings of the Ocean Drilling Program, Initial Reports, v. 146 (Part 1)*, ed.: Westbrook, G.K., Carson, B., and Musgrave, R.J., pp. 301-375, College Station, TX (Ocean Drilling Program), 1994.

Shrieve, Ronald L., Cloos, Mark, Dynamics of Sediment Subduction, Melange Formation, and Prism Accretion, *Journal of Geophysical Research,* v. 91, pp. 10,229-10,245, 1986.

Simpson, R.W., Cox, A., Paleomagnetic Evidence for Tectonic Rotation of the Oregon Coast Range, *Geology,* v. 5, pp. 585-589, 1977.

Snavely, P.D. Jr., Tertiary Geologic Framework, Neotectonics, and Petroleum Potential of the Oregon-Washington Continental Margin, in *Geology and Resource Potential of the Continental Margin of Western North America and Adjacent Ocean Basins - Beaufort Sea to Baja California,* Earth Science Series, v. 6, ed.: Scholl, D.W., Grantz, A., Vedder, J.G., pp. 305-335, Circum-Pacific Council for Energy and Mineral Resources, Houston, 1987.

Snavely, P.D. Jr., MacLeod, N.S., Wagner, H.C., Tholeiitic and Alkalic Basalts of the Eocene Siletz River volcanics, Oregon Coast Range, *Am. J. Sci.*, v. 266, pp. 454-481, 1968.

Snavely, P.D. Jr., Wagner, H.C., Lander, D.L., *Geologic Cross Section of the Central Oregon Continental Margin,* contribution of the Plate Tectonics Group, U.S. Geodynamics Committee, Geological Society of America, 1980.

Snavely, P.D. Jr., Wagner, H.C., Lander, D.L., Land-Sea Geologic Cross Section of the Southern Oregon Continental Margin, *Map I-1463, Miscellaneous Investigations Series,* U.S. Geological Survey, 1985.

Talwani, Manik, Heirtzler, J.R., Computation of Magnetic Anomalies Caused by Two-Dimensional Bodies of Arbitrary Shape, in *Computers in the Mineral Industries, Part 1,* ed.: G.A. Parks, v. 9, pp. 464-480, Stanford Univ. Publ., 1964.

Talwani, Manik, Worzel, J. Lamar, Landisman, Mark, Rapid Gravity Computations for Two-Dimensional Bodies with Application to the Mendocino Submarine Fracture Zone, *Journal of Geophysical Research,* v. 64, pp. 49-59, 1959.

Telford, W.M., Geldart, L.P., Sheriff, R.E., *Applied Geophysics*, 770 pp., Cambridge University Press, New York, 1990.

Thatcher, Wayne, Earthquake Recurrence and Risk Assessment in Circum-Pacific Seismic Gaps, *Nature,* v. 341, pp. 432-434, 1989.

Thatcher, Wayne, Order and Diversity in the Modes of Circum-Pacific Earthquake Recurrence, *Journal of Geophysical Research,* v. 95, pp. 2609-2623, 1990.

Trehu, A.M., Tracing the Subducted Crust Beneath the Central California Continental Margin: Results From Ocean Bottom Seismometers Deployed During the 1986 Pacific Gas and Electric EDGE Experiment, *Journal of Geophysical Research,* v. 96, pp. 6493-6506, 1991.

Trehu, A.M., Asudeh, I., Brocher, T.M., Luetgert, J.H., Mooney, W.D., Nabelek, J.L., Nakamura, Y., Crustal Architecture of the Cascadia Forearc, *Science*, v. 265, pp. 237-243, 1994.

Trehu, A.M., Lin, G., Maxwell, E., Goldfinger, C., A Seismic Reflection Profile Across the Cascadia Subduction Zone Offshore Central Oregon: New Constraints on Methane Distribution and Crustal Structure, *Journal of Geophysical Research,* v. 100, pp. 15,101-15,116, 1995.

Turcotte, Donald L., and Schubert, Gerald, *Geodynamics: Applications of Continuum Physics to Geological Problems,* 450 pp., John Wiley and Sons, New York, 1982.

von Huene, R., Pecher, I.A., Gutscher, M.-A., Development of the Accretionary Prism along Peru and Material Flux after Subduction of Nazca Ridge, *Tectonics*, v. 15, pp. 19-33, 1996.

Wang, K., Simplified Analysis of Horizontal Stresses in a Buttressed Forearc Sliver at an Oblique Subduction Zone, *Geophysical Research Letters,* v. 23, pp. 2021-2024, 1996.

Wang, Wei-Hau, and Davis, Dan M., Sandbox Model Simulation of Forearc Evolution and Noncritical Wedges, *Journal of Geophysical Research,* v. 101, pp. 11,329-11,339, 1996.

Webring, Michael, SAKI: A Fortran Program for Generalized Linear Inversion of Gravity and Magnetic Profiles, *Open File Report 85-122,* U.S. Geological Survey, 1985.

Wells, R.E., Engebretson, D.C., Snavely, P.D. Jr., Coe, R.S., Cenozoic Plate Motions and the Volcano-Tectonic Evolution of Western Oregon and Washington, *Tectonics,* v. 3, pp. 275-294, 1984.

Wells, R.E., Heller, P.L., The Relative Contribution of Accretion, Shear, and Extension to Cenozoic Tectonic Rotation in the Pacific Northwest, *Geological Society of America Bulletin,* v. 100, pp. 325-338, 1988.

Werner, K.S., Graven, E.P., Berkman, T.A., Parker, M.J., Direction of Maximum Horizontal Compression in Western Oregon Determined by Borehole Breakouts, *Tectonics*, v. 10, pp. 948-958, 1991.

Wessel, P., Smith, W.H.F., Free Software Helps Map and Display Data, *EOS Trans. AGU*, 72, p. 441, 1991.

Wilson, Douglas S., Tectonic History of the Juan de Fuca Ridge Over the Last 40 Million Years, *Journal of Geophysical Research,* v. 93, pp. 11,863-11,876, 1988.

Wilson, Douglas S., Confidence Intervals for Motion and Deformation of the Juan de Fuca Plate, *Journal of Geophysical Research,* v. 98, pp. 16,053-16,071, 1993.

Won, I.J., Bevis, Michael, Computing the Gravitational and Magnetic Anomalies due to a Polygon: Algorithms and Fortran Subroutines, *Geophysics*, v. 52, pp. 232-238, 1987.

Yeats, Robert S., Sieh, Kerry, Allen, Clarence R. *The Geology of Earthquakes*, Oxford University Press, New York, in press.

Zoback, Mary Lou, First- and Second-Order Patterns of Stress in the Lithosphere: The World Stress Map Project, *Journal of Geophysical Research,* v. 97, pp. 11,703-11,728, 1992.

APPENDIX

APPENDIX: COMPUTATIONAL BASIS FOR MAGNETICS AND GRAVITY MODELLING

Talwani, Worzel, and Landisman developed the mathematical basis for using a computer to calculate the gravitational attraction of a body in their seminal 1959 paper. This technique has been used in most, if not all, computer code subsequently written to perform two-dimensional gravity modelling and as a starting point for so-called two-and-a-half and two-and-three-quarters dimensional gravity modelling.

Talwani et al. (1959) used a n-sided polygon to approximate the cross-sectional shape of the body whose gravitational attraction is to be calculated (the polygon *ABCDE* in figure A.1). *P* is the origin of the *xz* coordinate system. The cross-section lies in the *xz* plane. *z* is defined positive downward, *x* is positive to the right, and θ is measured from the positive *x* axis to the positive *z* axis.

Hubbert (1948) showed that the vertical component of the gravitational attraction of a two-dimensional polygonal body, measured at the origin, *P*, is:

$$g_z = 2G\rho \oint z \, d\theta \qquad (A.1)$$

The line integral is taken along the sides of the polygon. Similarly, the horizontal component of the gravitational attraction of a two-dimensional body, measured at the origin, is:

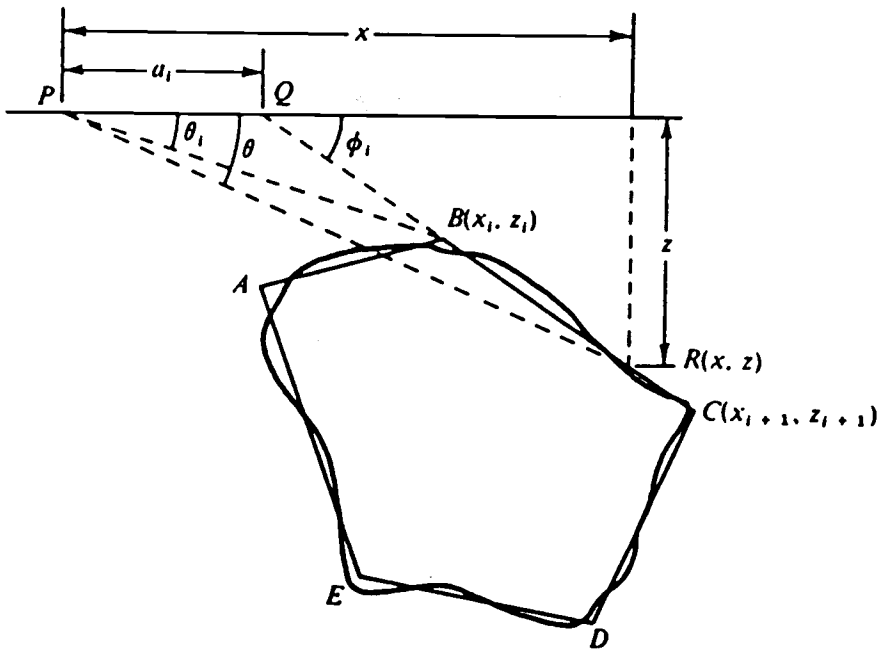

Figure A.1. Geometry used to derive the formulae for Telwani et al.'s method of forward gravity modelling (1959). (From Telford et al., 1990, p. 45)

$$g_x = 2G\rho \oint x \, d\theta \tag{A.2}$$

where G = universal gravitational constant and ρ = density of the polygon. Only the vertical component is considered in most gravity studies.

Consider the side BC of the polygon of figure A.1. The line CB contacts the x axis at an angle ϕ_i . Let R be a point lying at (x,z) on the line segment BC, and let the length of the line segment PQ have length a_i . Then for any arbitrary point R on BC:

$$z = x \tan\theta \tag{A.3}$$

and:

$$z = (x - a_i) \tan\theta \tag{A.4}$$

Combining equations A.3 and A.4, we obtain:

$$z = (a_i \tan\theta \tan\phi_i) / (\tan\phi_i - \tan\theta) \tag{A.5}$$

Subsituting equation A.5 into A.1, we find that the line integral over the line segment BC may be expressed in the form:

$$\int_{BC} z \, d\theta = \int_{BC} [(a_i \tan\theta \tan\phi_i) / (\tan\phi_i - \tan\theta)]d\theta = Z_i \qquad (A.6)$$

Similarly, the contribution of the line segment BC to the horizontal component of the gravitational attraction of the body is:

$$\int_{BC} x \, d\theta = \int_{BC} [(a_i \tan\phi_i) / (\tan\phi_i - \tan\theta)]d\theta = X_i \qquad (A.7)$$

The vertical and horizontal components of the gravitational acceleration due to the body outlined by the polygon $ABDCDE$, measured at P, are, respectively:

$$g_z = 2G\rho \sum_{i=1,n} Z_i \qquad (A.8)$$

and:

$$g_x = 2G\rho \sum_{i=1,n} X_i \qquad (A.9)$$

where n = the total number of sides of the polygon. Solving the integrals for Z_i and X_i, we obtain:

$$Z_i = a_i \sin\phi_i \cos\phi_i \{\theta_i - \theta_{i+1} + \tan\phi_i \log_e [(\cos\theta_i (\tan\theta_i - \tan\phi_i)) / (\cos\theta_{i+1} (\tan\theta_{i+1} - \tan\phi_i))]\} \qquad (A.10)$$

$$X_i = a_i \sin\phi_i \cos\phi_i \{\tan\theta_i \ (\theta_{i+1} - \phi_i) + \log_e [(\cos\theta_i \ (\tan\theta_i - \tan\phi_i)) / (\cos\theta_{i+1} \ (\tan\theta_{i+1} - \tan\phi_i))]\} \quad (A.11)$$

where:

$$\theta_i = \tan^{-1} (z_i / x_i) \quad (A.12)$$

$$\phi_i = \tan^{-1} [(z_{z+1} - z_i) / (x_{i+1} - x_i)] \quad (A.13)$$

$$\theta_{i+1} = \tan^{-1} (z_{i+1} / x_{i+1}) \quad (A.14)$$

and:

$$a_i = x_{x+1} + z_{i+1} [(x_{i+1} - x_i) / (z_i - z_{i+1})] \quad (A.15)$$

The gravitational attraction of the body may thus be calculated from only its density and the locations of the vertices of the polygon used to approximate it. By using a polygon with a large number of sides, complicated body geometries may be modelled. As the gravitational effects of multiple bodies add by superposition, the response of a complex model may be calculated by performing the above procedure for each model body and summing the results. The simple but multitudinous calculations required are ideally suited to the use of a computer.

Similarly, techniques used for computer-based forward magnetic modelling also use a polygon to approximate a two-dimensional anomalous body. Talwani and Heirtzler (1964) approached the problem by dividing an infinite polygonal cylinder into semi-infinite horizontal slabs, each bounded by one of the polygon's sides, and combining the magnetic anomalies due to each. An alternate method suggested by Won and Bevis (1987) makes use of Poisson's relation, which relates the gravitational effect of an anomalous body to its magnetic response. Poisson's relation is also used to construct pseudogravity maps. If the gravitational attraction of a body is known, then Poisson's relation may be used to calculate its magnetic response. Applying Poisson's relation to the vertical and horizontal components of the magnetic and gravitational fields, respectively, we obtain:

$$H_z = [(k H_e) / (G \rho)] (\partial g_z / \partial \alpha) \qquad (A.16)$$

and:

$$H_x = [(k H_e) / (G \rho)] (\partial g_x / \partial \alpha) \qquad (A.17)$$

where k = magnetic susceptibility of the polygon, H_e = ambient scalar earth magnetic field strength, G = universal gravitational constant, ρ = density of the polygon, and α = the direction of induced magnetization. It is assumed that remnant magnetization is negligible. It can also be shown that:

$$\partial / \partial\alpha = (\sin I)(\partial / \partial z) + (\sin \beta)(\cos I)((\partial / \partial x) \quad (A.18)$$

where I = geomagnetic field inclination, and β = strike of the polygonal cylinder measured counterclockwise from magnetic north to the negative y axis. Detailed expressions for the derivates in terms of simple model geometry parameters, similar to those outlined for the forward gravity modelling method, are given in Won and Bevis. g_z and g_x may be obtained using the method of Talwani et al. (1959) described above.

Unlike most gravity studies, the magnitude of the total field rather than just that of the vertical component is typically considered in magnetic modelling. The total field scalar anomaly is given by:

$$H = (H_z)(\sin I) + (H_x)(\sin \beta)(\cos I) \quad (A.19)$$

Inversion consists of an algorithm that compares the difference between observed and calculated values of some quantity, such as the gravitational or magnetic field, and attempts to minimize that error through iterative adjustment of model parameters, such as density, magnetic susceptibility, or the locations of vertices of the polygon used to approximate the cross-sectional geometry of an anomalous body (Telford et al., 1990, p. 123). It was found that geologically realistic modelling results were more consistently and easily obtained by manually adjusting the model parameters between forward modelling runs, using judgement and experience rather than the automated inversion capabilities of the software. Inversion was only used to provide starting

values for certain model parameters, including the susceptibility of the Siletz terrane, which were subsequently modified by the user during an iterative forward modelling process. As inversion techniques are highly complex, and as the inversion capabilities of the GM-SYS package were not extensively used, they will not be discussed here in detail. A description of the mathematical techniques used to invert gravity and magnetics data in the U.S. Geological Survey's SAKI code is given in Webring (1985), and a more thorough treatment of the subject is given in Parker (1994).